To the Graduate Council:

I am submitting herewith a thesis written by Vicki Jo Brumback entitled "A Metamorphic and Structural Transect in the Central Blue Ridge, Jackson and Macon Counties, North Carolina." I have examined the final copy of this thesis for form and content and recommend that it be accepted in partial fulfillment of the requirements for the degree of Master of Science, with a major in Geology.

Harry Y. McSween, Jr., Major Professor

We have read this thesis
and recommend its acceptance:

Accepted for the Council:

Vice Provost
and Dean of The Graduate School

STATEMENT OF PERMISSION TO USE

In presenting this thesis in partial fulfillment of the requirements for a Master's degree at the University of Tennessee, Knoxville, I agree that the Library shall make it available to borrowers under rules of the Library. Brief quotations from this thesis are allowable without special permission, provided that accurate acknowledgment of the source is made.

Permission for extensive quotation from or reproduction of this thesis may be granted by my major professor, or in his absence, by the Head of Interlibrary Services when, in the opinion of either, the proposed use of the material is for scholarly purposes. Any copying or use of the material in this thesis for financial gain shall not be allowed without my written permission.

Signature Vicki Jo Brumbach

Date November 26, 1990

A METAMORPHIC AND STRUCTURAL TRANSECT IN THE CENTRAL BLUE RIDGE, JACKSON AND MACON COUNTIES, NORTH CAROLINA

A Thesis

Presented for the

Master of Science

Degree

The University of Tennessee, Knoxville

Vicki Jo Brumback

December 1990

ACKNOWLEDGMENTS

A special thanks goes to Dr. Hap McSween who served as my major advisor and suggested this thesis project in the fascinating Blue Ridge. He provided much needed guidance and enthusiasm throughout the project. I would also like to thank the other members of my committee, Dr. Ted Labotka and Dr. Bob Hatcher, for their advice, constructive criticism, and support. Other faculty members in the Geology Department and fellow students/friends increased my knowledge in and enhanced my appreciation of the field of geology, and I value the time I spent in the master's program.

In addition, I would like to thank my friends in the Office of Risk Analysis at Oak Ridge National Laboratory for their encouragement and assistance. Gloria and Fred Hinson of Cullowhee, North Carolina opened their home to me during my field work, and are friends "in deed". Finally, I thank my family and J.C. Their love and inspiration are foundational to anything I do.

ABSTRACT

A Late Proterozoic metamorphic terrane in the central Blue Ridge of western North Carolina preserves a nearly continuous record of regionally metamorphosed high-pressure facies rocks ranging from amphibolite to granulite facies. A wide variety of lithologic types in the stratigraphic units (Copperhill Formation/Ocoee Series, Tallulah Falls Formation, and Otto Formation) of the study area allows documentation of metamorphic conditions across this boundary.

Petrographic study indicates that the following metamorphic zones occur in the study area: (1) the first-sillimanite zone, (2) the second-sillimanite zone (first appearance of sillimanite + K-feldspar) in association with partial melting in pelites, and (3) the hypersthene zone (hornblende + orthopyroxene + clinopyroxene + garnet) in amphibolites. The second-sillimanite isograd is constrained along strike approximately 5 km northeast of Franklin, defining the northern extent of the granulite facies thermal core.

Phase relations and mineral exchange equilibria place the assemblages of the amphibolite facies at 550-600 °C and 5.5-6 kbar, and assemblages of the granulite facies at 670-800 °C and >7.5 kbar.

In addition, pre- to syn- (Hayesville) to post-metamorphic-peak (Soque River) faults juxtapose terranes of different metamorphic grade, allowing delineation of the

timing of deformation relative to metamorphism. The presence of these thrust faults in the area emphasizes the effect that overthrusting had on burial depth and formation of high temperature and pressure metamorphic conditions.

TABLE OF CONTENTS

CHAPTER			PAGE
CHAPTER	1.0	INTRODUCTION	1
	1.1	Introduction and Purposes of Study . . .	1
	1.2	Regional Geology	5
	1.3	Methods	12
CHAPTER	2.0	CHARACTERIZATION OF DEFORMATION	14
	2.1	Megascopic Structure	14
	2.2	Mesoscopic Structures and Microscopic Textures	23
CHAPTER	3.0	PETROGRAPHY AND MINERAL ASSEMBLAGES OF STUDY AREA LITHOLOGIES	38
	3.1	Ocoee Series/Great Smoky Group	39
	3.2	Tallulah Falls Formation	43
	3.3	Otto Formation	53
	3.4	Mineral Chemistry	60
		3.4.1 Pelitic rocks	60
		3.4.2 Amphibolitic rocks	62
CHAPTER	4.0	REACTIONS AND CONDITIONS OF METAMORPHISM	66
	4.1	Isograds and Metamorphic Reactions . . .	66
	4.2	Compositional Diagrams and Projections	68
	4.3	Pressure and Temperature Indicators	71
		4.3.1 Pressure and Temperature from Reaction Relationships	71
		4.3.2 Temperature Calculations from Mineral Exchange Equilibria Calculations	73
CHAPTER	5.0	CONCLUSIONS	81
LIST OF REFERENCES			83
APPENDIX			91
VITA			103

LIST OF TABLES

TABLE		PAGE
Table 1.	Garnet-biotite temperature estimates (in °C) for both garnet core-biotite matrix and garnet rim-adjacent biotite associations	75
Table A.1.	Representative garnet analyses in pelitic rocks	93
Table A.2.	Representative biotite analyses in pelitic rocks	95
Table A.3.	Representative muscovite analyses in pelitic rocks	97
Table A.4.	Representative plagioclase and K-feldspar analyses in pelitic rocks . .	98
Table A.5.	Representative staurolite analyses in pelitic rocks	99
Table A.6.	Representative hornblende (hb) and biotite (bi) analyses in amphibolitic rocks	100
Table A.7	Representative garnet (grt) and pyroxene (px) analyses in amphibolitic rocks	101
Table A.8	Representative plagioclase analyses in amphibolitic rocks	102

LIST OF FIGURES

FIGURE		PAGE
Figure 1.	Location of the study area relative to well-known features of the southern Appalachians (modified from Eckert et al., 1989)	3
Figure 2.	Locations and names of quadrangles in the vicinity of the study area.	8
Figure 3.	Regional and deformational events sequence from Absher and McSween (1985).	15
Figure 4.	Hand samples showing increasing deformation of the Copperhill Formation of the Ocoee Series nearing the Hayesville Fault.	18
Figure 5.	Photomicrograph of deformed Copperhill Formation schist (sample K04F).	19
Figure 6.	Outcrop photograph showing crenulations in the Ocoee Series near the Hayesville Fault.	20
Figure 7.	Photomicrograph of crenulation.	21
Figure 8.	Upright F_3 fold in the Tallulah Falls Formation exposed in the town of Dillsboro.	26
Figure 9.	Fold generation in the Otto Formation at the Tathams Creek outcrop.	27
Figure 10.	Undeformed pegmatite dikes.	30
Figure 11.	Mylonite in outcrop.	31
Figure 12.	Mylonite hand sample.	32
Figure 13.	Mylonite photomicrograph.	33
Figure 14.	Mylonite hand sample.	34
Figure 15.	Mylonite photomicrograph.	35

LIST OF FIGURES (continued)

FIGURE		PAGE
Figure 16.	Photomicrograph of Copperhill Formation metagraywacke showing typical mosaic of quartz, plagioclase, and biotite.	41
Figure 17.	Photomicrograph of Copperhill Formation schist.	42
Figure 18.	Tallulah Falls Formation sample from northern end of the study area.	45
Figure 19.	Photomicrograph of the Tallulah Falls Formation.	46
Figure 20.	Tallulah Falls Formation biotite gneiss from the southern part of the study area.	47
Figure 21.	Photomicrograph of partial melt bleb (bottom half)	48
Figure 22.	Tallulah Falls Formation biotite gneiss showing increased grain size. . .	49
Figure 23.	Photomicrograph of Tallulah Falls Formation biotite gneiss under granulite facies.	50
Figure 24.	Otto Formation at the Tathams Creek location.	54
Figure 25.	Photomicrograph of the Otto Formation gneiss.	55
Figure 26.	Otto Formation gneiss and amphibolite in upright F_3 fold.	56
Figure 27.	Photomicrograph of Otto Formation showing and amphibolite fold nose. . . .	57
Figure 28.	Photomicrograph of the aluminous schist member of the Otto Formation. . .	58
Figure 29.	Garnet composition.	63

LIST OF FIGURES (continued)

FIGURE		PAGE
Figure 30.	AFM projections (after Thompson, 1957) for pelitic rocks.	70
Figure 31.	Relevant mineral equilibria for the pressure and temperature conditions of medium-to high-grade metamorphism for study area assemblages.	72
Figure 32.	Estimated temperatures using mineral exchange equilibria equations.	79

LIST OF PLATES

Plate . . . . . In Pocket

CHAPTER 1.0

INTRODUCTION

1.1 Introduction and Purposes of Study

A metamorphic terrane in the eastern Blue Ridge of the southern Appalachians has been recognized in previous studies as part of a progressive Barrovian sequence, ranging up through the second-sillimanite zone and hornblende granulite subfacies of the granulite facies (Carpenter, 1970; Hadley and Nelson, 1971; Eckert et al., 1989). A granulite-facies metamorphic core has been identified in southwestern North Carolina (Force, 1976; Hatcher and Butler, 1979), with progressively lower grades occurring along the flanks of the core. This range in metamorphic grade was likely produced by a single Paleozoic (Taconian) metamorphic event (Butler, 1972; Butler, 1973; Dallmeyer, 1975; Hatcher and Butler, 1979; Glover et al., 1983; Absher, 1984; Absher and McSween, 1985; Kittleson, 1988; Eckert et al., 1989).

Most exposed high-grade Barrovian terranes are Precambrian (Bohlen, 1983) and have complex thermal and deformational histories. Constraints on high-grade metamorphic conditions and the timing of deformation are problematic due to the widespread presence of disequilibrium assemblages, retrograde effects, and complex structural relationships. Previous studies of this relatively young high-grade terrane in the Blue Ridge, however, have shown that

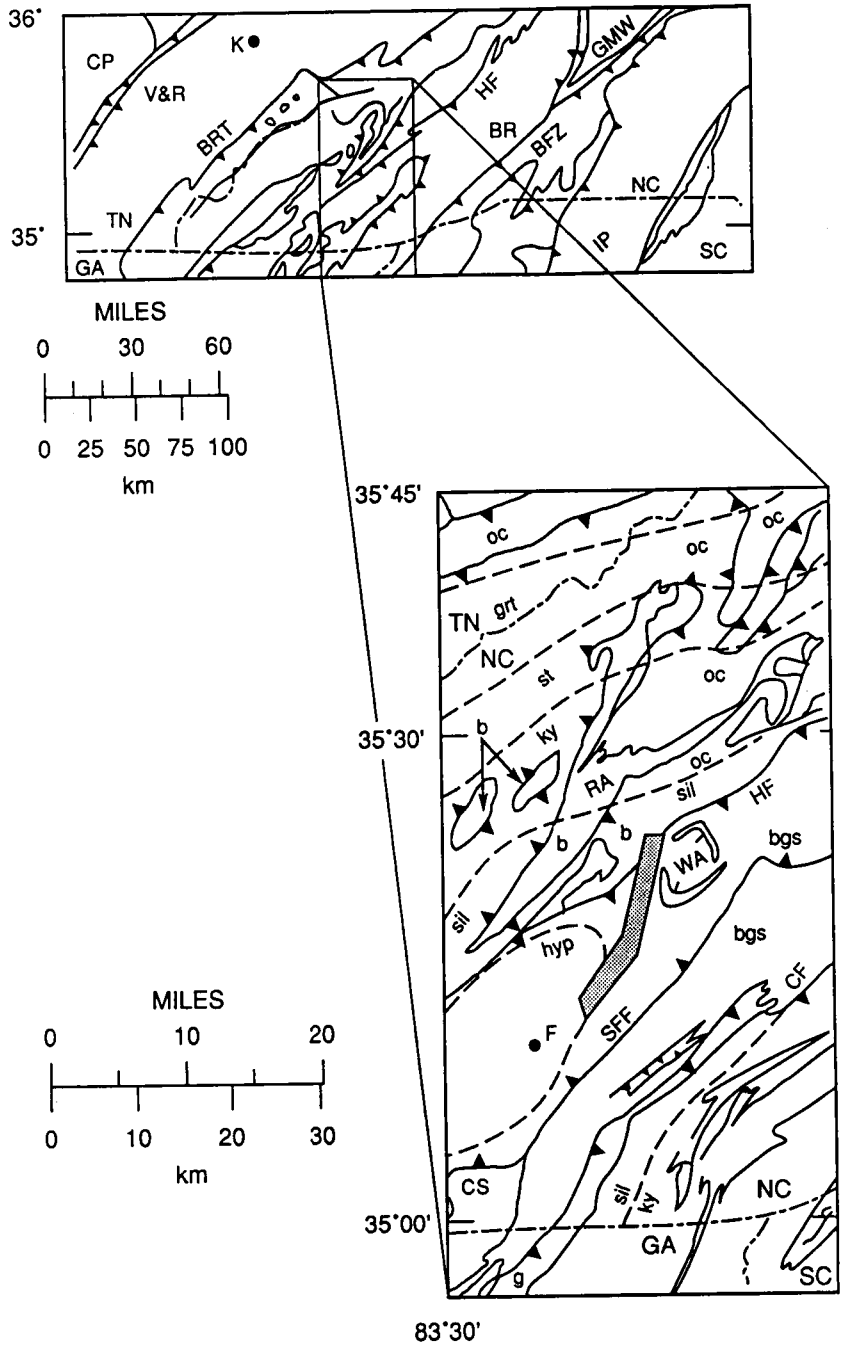
retrograde effects are limited (Absher and McSween, 1985; Kittleson, 1988; Eckert et al., 1989). Thus, this area offers a rare opportunity to determine more accurately the conditions necessary for the development of high-grade metamorphism. The diverse lithologies present in this area (i.e., interlayered biotite gneiss, mica schist, and amphibolite) aid in defining the metamorphic conditions. Furthermore, quantification of changing metamorphic conditions at the transition from lower-grade to higher-grade facies in this area provides a greater understanding of the thermal history of the Blue Ridge and, along with other studies, provides information on the tectonic development of the region.

This study focuses on an along-strike geologic transect (Figure 1) that reveals the prograde character of the terrane, details mesoscopic structural features, and also crosses a major pre- to syn-metamorphic-peak tectonostratigraphic boundary, the Hayesville Fault (Hatcher, 1978). Previous studies to the south, (described in more detail in Section 1.2) have mapped across the short axis of the thermal core, fixing the locations of isograds and major structural features (Kittleson, 1988; Eckert et al., 1989). This study will complement the previous work by locating isograds and structural features north of the thermal core. This study will also address the relationship between the metamorphic environment and structural features and will attempt to correlate structural features in the study

Figure 1. Location of the study area relative to well-known features of the southern Appalachians (modified from Eckert et al., 1989). The study area is the shaded corridor on the large-scale map.

ON SMALL-SCALE MAP ONLY: Cumberland Plateau (CP); Valley and Ridge belt (V&R); Blue Ridge thrust (BRT); Blue Ridge belt (BR); Grandfather Mountain Window (GMW); Inner Piedmont (IP); Brevard Fault Zone (BFZ). Knoxville, Tennessee, also is shown (filled circle, K).

ON LARGE-SCALE MAP: Ravensford anticline (RA); Coweeta syncline (CS); Hayesville fault (HF); Shope Fork fault (SFF). Lithologic subdivisions: Ocoee Series, including the Great Smoky Group (oc); Grenville basement rocks (b); biotite gneiss and schist of the Piedmont terrane (bgs); Webster-Addie Complex (WA). Franklin, North Carolina, also is shown (filled circle, F). Isograds: Dashed lines, designated for first appearance of index minerals. (Reconnaissance observations indicate that the "hypersthene zone" as drawn extends too far to the northeast (Eckert, 1988).) Mineral abbreviations: hypersthene (hyp), garnet (grt), sillimanite (sil), staurolite (st), and kyanite (ky).


36°
35°
CP
K
V&R
BRT
TN
GA
HF
GMW
BR
BFZ
NC
IP
SC
MILES
0 30 60
0 25 50 75 100
km
35°45'
35°30'
35°00'
83°30'
oc
TN
grt
NC
st
ky
b
RA
sil
HF
WA
bgs
hyp
F
SFF
CF
CS
g
GA
SC
MILES
0 10 20
0 10 20 30
km

area with the comprehensive sequence of deformation events already established in previous studies. This work, along with work in progress in nearby areas, will fill in details in an area heretofore mapped only at a small scale.

The study area covers portions of the Whittier, Greens Creek, and Corbin Knob 7.5 minute quadrangles in Jackson and Macon counties, western North Carolina (Plate, In Pocket). The study area is approximately 24 kilometers long by 3 kilometers wide and covers approximately 72 square kilometers between the towns of Dillsboro and Franklin. This study area was chosen along Highway 441/23 because of newly constructed roadcuts.

1.2 Regional Geology

The Blue Ridge physiographic province is basically a structural block of metaigneous and metasedimentary rocks, separated from the Valley and Ridge thrust belt in the west by the Blue Ridge thrust fault zone and from the Inner Piedmont in the east by the Brevard fault system (Figure 1, small-scale map). Geological and geophysical data suggest that the Blue Ridge along with the Inner Piedmont is part of a large thrust sheet (Hatcher, 1972; Hatcher and Zietz, 1979; Cook et al., 1979) that was involved in many episodes of movement over much of the Paleozoic. This movement occurred along a master décollement extending under the Blue Ridge, possibly to the Coastal Plain, on which a minimum estimate of transport is 260 km (Cook et al., 1979). Windows (e.g., Grandfather Mountain

Window, Figure 1, large-scale map), in which low-grade rocks are exposed under higher-grade rocks, also indicate that the Blue Ridge is allochthonous.

The Blue Ridge in western North Carolina has been divided into two lithotectonic belts separated by the Hayesville fault (Hatcher, 1978; Hatcher et al., 1979). The eastern Blue Ridge contains metasedimentary, volcanic, and ultramafic rocks ("oceanic terrane"), whereas the western Blue Ridge contains late Precambrian metasedimentary rocks of the Ocoee Series and Grenville basement with few mafic or ultramafic rocks ("continental terrane") (Rankin, 1975; Hatcher, 1978). Most of the study area is located in the eastern Blue Ridge, but the northern end of the transect crosses the Hayesville fault into rocks of the Ocoee Series.

The differences between the eastern and western Blue Ridge have been interpreted as a break between continental shelf deposits of the western Blue Ridge and deeper-water, rift-related sediments of the eastern Blue Ridge, with mafic and ultramafic rocks representing possible dismembered ophiolites (Hatcher et al., 1984; McSween and Hatcher, 1985). (Areal distribution of the ultramafic bodies has been mapped by Larrabee (1966), and Figure 1 shows the location of the Webster-Addie ultramafic body to the east-northeast of the study area.) Raymond et al. (1988) have recently proposed a mélange origin as an alternative for the rocks in the eastern terrane. Their proposal is based on the presence of

ultramafic rocks, evidence of pre-peak-metamorphic fragmentation, and possible "block-in-matrix" structures found in this area of the Blue Ridge.

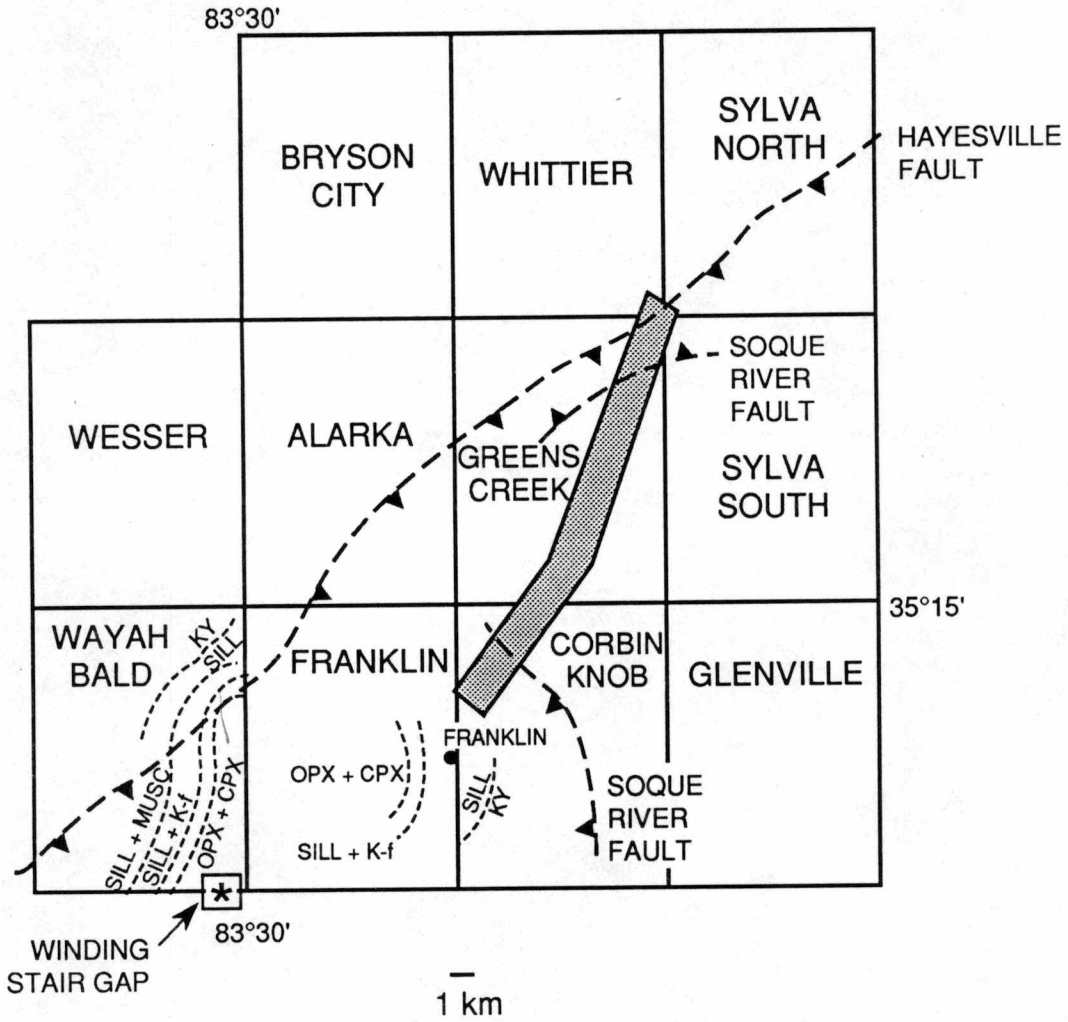
Granitic gneiss and biotite schist are the dominant rock types in the study area, but migmatites, mylonites, and orthoamphibolites are common. Figure 1 shows the generalized geology in the vicinity of the study area, and the caption provides part of the stratigraphy of the Blue Ridge in the Appalachians, modified from Eckert et al. (1989). Figure 2 shows the locations and names of quadrangles in the vicinity of the study area.

Hadley and Nelson (1971) described the rocks in this area as biotite schist, gneiss, and migmatite of Middle and Upper Precambrian age in their geologic map of the Knoxville quadrangle. Hatcher and Butler (1979) tentatively correlated the rocks in the "eastern" area with either the Tallulah Falls Formation or the Coweeta Group. Study of an adjacent area left the correlation as Tallulah Falls Formation/Coweeta Group undivided (Kittleson, 1988), but recent work to the east (M. Quinn, pers. comm.) has refined the correlation to the Tallulah Falls and Otto Formations. The Tallulah Falls Formation, in general, is composed of metamorphosed pelitic and mafic volcanic rocks (Hatcher, 1973), and the Otto Formation is a sequence of relatively quartz-rich two-mica feldspathic sandstone interlayered with aluminous schist (Hatcher, 1988).

Figure 2. Locations and names of quadrangles in the vicinity of the study area. The study area is the shaded corridor. Mapping credits are as follows:

Kittleson (1988)	southern half of the Corbin Knob quadrangle and southeastern portion of the Franklin quadrangle (Isograds shown are (1) sillimanite, (2) K-feldspar + sillimanite, and (3) orthopyroxene + clinopyroxene)
Quinn (in prep.)	southern portion of the Sylva North quadrangle and northern portion of the Sylva South quadrangle
Shireman, et al. (1985)	Sylva South quadrangle
Eckert (1988)	eastern half of the Wayah Bald quadrangle (Isograds shown are (1) sillimanite, (2) sillimanite + muscovite, (3) sillimanite + K-feldspar, and (4) orthopyroxene + clinopyroxene)
Absher (1984)	Winding Stair Gap and vicinity (star in southeastern corner of the Wayah Bald quadrangle)

In addition, the entire area shown was included by Hadley and Nelson (1971).


83°30'
BRYSON CITY
WHITTIER
SYLVA NORTH
HAYESVILLE FAULT
SOQUE RIVER FAULT
WESSER
ALARKA
GREENS CREEK
SYLVA SOUTH
35°15'
WAYAH BALD
KY SILL
FRANKLIN
CORBIN KNOB
GLENVILLE
FRANKLIN
OPX + CPX
SILL + K-f
SILL KY
SOQUE RIVER FAULT
SILL + MUSC
SILL + K-f
OPX + CPX
83°30'
WINDING STAIR GAP
1 km

Eckert (1984) correlated rocks in the high-grade metamorphic core with the Coweeta Group and Tallulah Falls Formation, and also delineated a series of prograde metamorphic zones from northwest to southeast into the metamorphic core: kyanite + muscovite, sillimanite + muscovite (or first-sillimanite zone), sillimanite + K-feldspar (or second-sillimanite zone), and the coexistence of orthopyroxene and clinopyroxene in mafic rocks (granulite zone). In a follow-up study, Eckert et al. (1989) have shown that the metamorphic progression into the granulite core is continuous across the Hayesville fault. This study looks at the progression into the core along strike and includes the northeastern tip of the second-sillimanite zone which was originally delineated by Force (1976).

Absher and McSween (1985) determined peak metamorphic conditions at Winding Stair Gap in the metamorphic core to be approximately 750 °C and 6.5 kbar. Kittleson (1988) estimated conditions of metamorphism at 500-680 °C and 5.5-6.8 kbar in the amphibolite facies, and 680-780 °C and 6.5-8.0 kbar in the granulite facies. Eckert et al. (1989) found peak metamorphic conditions in the hornblende granulite facies of the core to be 842 °C and 9.8 kbar. Temperature calculations using data from rocks in the field area are provided in Chapter 4.

The age of metamorphic and deformational events can be determined using isotopic, structural, and petrologic data. Radiometric age dating has placed the main metamorphic event

at 480-430 Ma, Early Ordovician or Early Silurian (Butler, 1972; Dallmeyer, 1975). A sample from Gay, N.C. (located in the study area), gave an age of 440 Ma using Rb-Sr dating techniques (Long et al., 1959). The Ordovician-Early Silurian ages have been correlated with the Taconian orogeny (Butler, 1973; Glover et al., 1983). Later regional deformational events were at 380-340 Ma (Devonian to early Mississippian), and 330-230 Ma (late Mississippian to Permian), which have been related to the Acadian and Alleghanian orogenies, respectively (Butler, 1973; Glover et al., 1983). The timing of deformational events will be discussed in more detail in Chapter 2.

Most studies in this area have delineated the metamorphic isograds by identification of index minerals. In addition, a study by Kittleson (1988) along a roughly east-west (across-strike) transect through the town of Franklin considered the bulk chemistry of the rocks and reactions that produced the observed mineral assemblages. As stated previously, this study will look at an along-strike transect from the northern extent of the granulite core across the Hayesville fault into the Ocoee rocks just northwest of Dillsboro. It intersects Kittleson's transect and complements his approach in extending a transect generally along strike in an attempt to establish trends north of the thermal core in this terrane. As in Kittleson's study, the boundary between the amphibolite and the granulite facies has been placed at the second sillimanite

isograd (i.e., the muscovite breakdown reaction to sillimanite plus K-feldspar). "Low grade" here refers to rocks that contain muscovite or are in the area of muscovite-bearing assemblages, and "high grade" refers to rocks that contain K-feldspar and sillimanite or are in the vicinity of K-feldspar- and sillimanite-bearing assemblages. Most of the study area lies within the amphibolite facies.

To aid in describing metamorphic trends into the high-grade core, four aspects of the petrogenesis are presented. First, the equilibrium mineral assemblages have been determined in order to confirm or establish the facies types. Second, temperature values are estimated for the assemblages to determine the metamorphic environment. Third, a reaction series is proposed to describe the pertinent isograds. Mineral reactions that are inferred to have occurred based on an AFM projection are also used to estimate the conditions of metamorphism.

1.3 Methods

Field work in the Whittier, Greens Creek, and Corbin Knob quadrangles was carried out on the scale of 1:24,000 utilizing 7.5 minute topographic sheets. Mapping consisted of one major transect through the study area following large exposures along U.S. Highway 441/23. Narrow across-strike transects utilized side roads and drainages. Sample locations are shown on the Plate (In Pocket), and petrographic descriptions of the stratigraphic units are given in Chapter 3. Representative

orientations of compositional layering and fold axes were measured and are also shown on the Plate (In Pocket). Approximately 200 thin sections were made, cut perpendicular to foliation, for study in transmitted light. Thirteen polished thin sections selected from the various lithologies and progressive metamorphic zones were studied using the electron microprobe.

Mineral compositions were quantitatively determined using a three-spectrometer Material Analysis Corporation (MAC) 400S automated electron microprobe with appropriate natural and synthetic standards. Data reduction utilized the correction scheme of Bence and Albee (1968) with the theoretical correction data of Albee and Ray (1970). Standard operating conditions were 15 keV accelerating potential for 20 seconds or 20,000 counts. A beam current of 0.05 μA with a beam diameter of 1 micron was used for analyzing garnet and pyroxene. A current of 0.03 μA with a defocused beam was used for analyzing biotite, feldspar, muscovite, and hornblende. Multiple analyses of grain cores and rims in several areas within each thin section were used to assess instrument precision, to document grain zonation in most samples, and to determine compositional ranges within the area of a thin section. Representative mineral analyses used in temperature calculations are given in the Appendix and are further discussed in Chapter 4.

CHAPTER 2.0

CHARACTERIZATION OF DEFORMATION

The interpretation of multiply deformed and metamorphosed terranes, such as the one in the study area, can be difficult because of the lack of distinct and continuous marker horizons. It is useful in studying such complex terranes to establish a relative sequence of deformational events for the area based on the correlation of structural features between exposures and on mesoscopic-scale overprinting features. Once this sequence has been established, relative and absolute dating techniques can be incorporated to place the deformational events onto a geologic time scale and discern regional trends. A "deformational event" is defined as any structural, intrusive, and/or metamorphic event that affected the terrane and is recorded by such features as faults, folds, foliations, and metamorphic mineral assemblages.

A regional metamorphic and deformational event sequence previously summarized in other studies is presented in Figure 3. In the remainder of this chapter, structural features observed in the study area will be correlated with this sequence, indicating that the features in the study area formed as a result of regional events.

2.1 Megascopic Structure

The Blue Ridge in western North Carolina is dominated by westward-vergent nappes and thrusts of a variety of ages

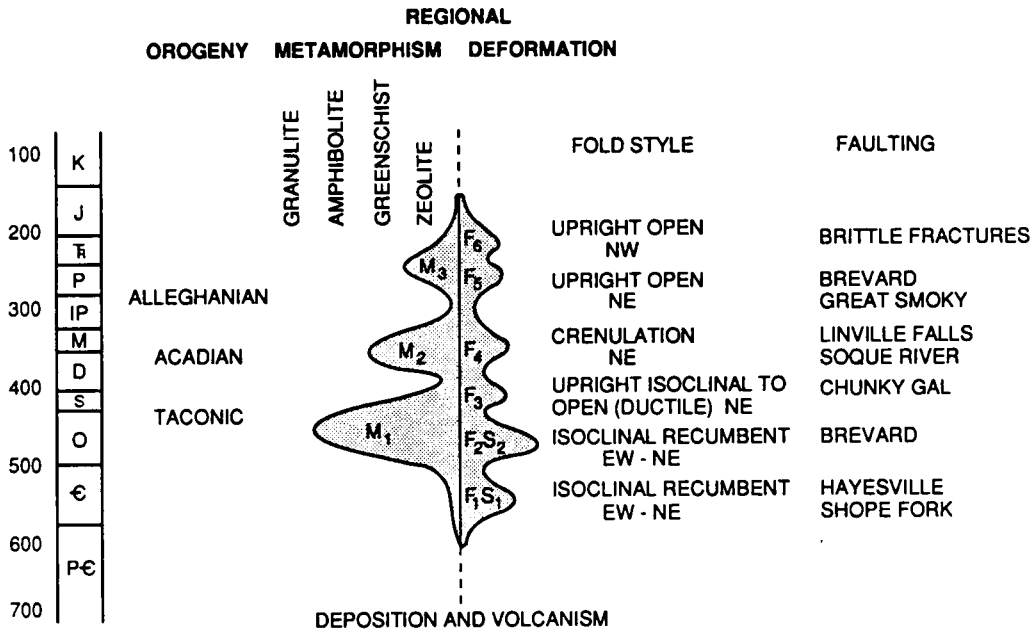


Figure 3. Regional metamorphic and deformational events sequence from Absher and McSween (1985). (Synthesized from Hatcher and Butler (1979), Hatcher et al., (1980), Butler and Fullager (1982), and Glover et al., (1983). Many of the inferred regional events have been documented only in localized areas outside the Blue Ridge, and not all events were observed in the study area.)

(i.e., from pre- to post-metamorphic-peak faults) (Hopson, et al., 1989).

The trace of the Hayesville fault lies in the northern part of the study area and trends to the northeast (Figure 1; Plate, In Pocket). It has been suggested that the Hayesville is a fundamental boundary within the Blue Ridge (Hatcher, 1978) and may be a cryptic suture rejoining fragmented segments of the ancient continental margin of North America (Hatcher et al., 1979). It has been identified as a pre-metamorphic suture which has transported older rocks over relatively younger rocks. The pre-metamorphic age of the fault has been confirmed by Eckert et al. (1989), who mapped isograds transecting the Hayesville Fault.

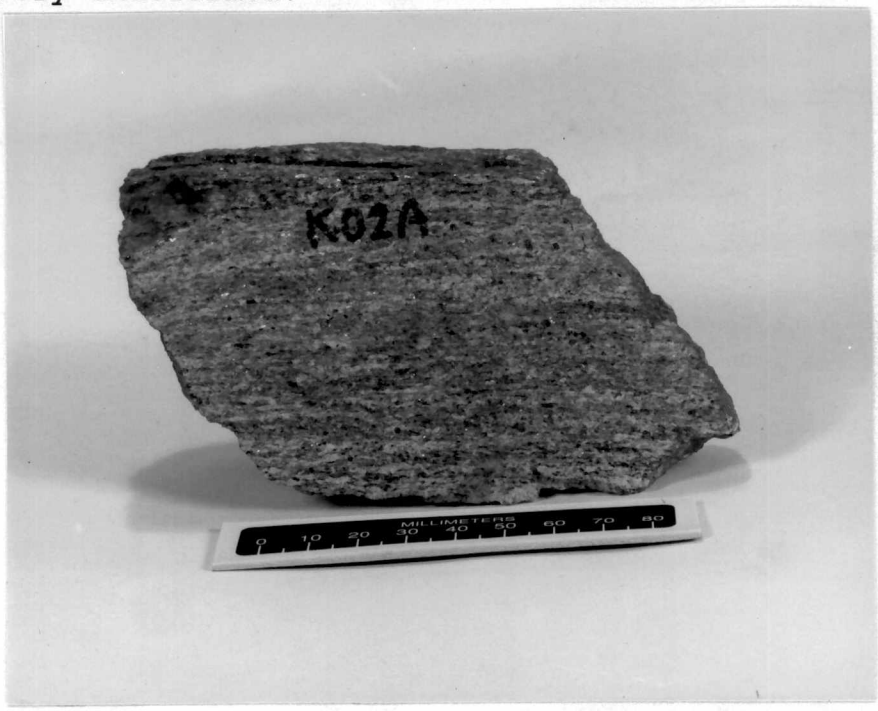
In the study area, the Hayesville fault places Middle and Upper Proterozoic-age rocks of the Tallulah Falls Formation over Upper Proterozoic-age Ocoee Series rocks of the Copperhill Formation-Great Smoky Group. The best exposure of the fault zone is in a roadcut in the community of Dillsboro (location J22, Plate, In Pocket). The placement of the fault zone was determined by the presence of a deformed exposure of Ocoee rocks and a nearby exposure of Tallulah Falls Formation rocks (separated by approximately 2000 ft). Because of the lack of deformed or mylonitized rocks in the hanging wall (Tallulah Falls Formation), I propose that the Hayesville began as a single fault and selectively incorporated the more incompetent Ocoee rocks into the fault. Figures 4 and 5 show

increasing deformation of Ocoee rocks into the fault zone. Figures 6 and 7 show crenulations in the muscovite schist of the Copperhill Formation, which may be related to a later deformational event. Near the fault, rocks of the Copperhill Formation of the Ocoee Series strike N64E and dip 64S. Fold axes (including the small crenulations shown in Figures 6 and 7) plunge to the southeast.

The Hayesville fault in the study area abruptly juxtaposes migmatitic metamorphic rocks (Tallulah Falls Formation) with metamorphic rocks that contain relict sedimentary structures (Copperhill Formation), suggesting telescoping of metamorphic "grade" along the fault, at least in this area, although both formations are thought to be in the first-sillimanite zone of the amphibolite facies. This would mean that some movement along the fault occurred during or after peak metamorphism. This different interpretation could be the result of variations of fault movement over time.

The Soque River fault is also mapped in the study area, juxtaposing the older higher-grade Tallulah Falls Formation and the tectonically lower younger Otto Falls Formation which contains lower-grade assemblages (Plate, In Pocket). Gillon (1982) and Nelson (1982) first recognized this fault as bounding the northwest margin of the Dahlonega gold belt in northern Georgia and proposed it to be a continuation of the Shope Fork fault. The Soque River fault was later named by Hatcher et al. (1987b). The placement of the Soque River

Figure 4. Hand samples showing increasing deformation of the Copperhill Formation of the Ocoee Series nearing the Hayesville fault. Nearby exposure of Tallulah Falls Formation is relatively undeformed.



a. Sample K02A shows typical relatively undeformed Copperhill Formation schist.



b. Sample K04F showing Copperhill Formation schist which has been mylonitized. (Figure 5 is a photomicrograph of sample K04F.)



Figure 5. Photomicrograph of deformed Copperhill Formation schist (sample K04F). Width of the photograph is approximately 1.5 mm.

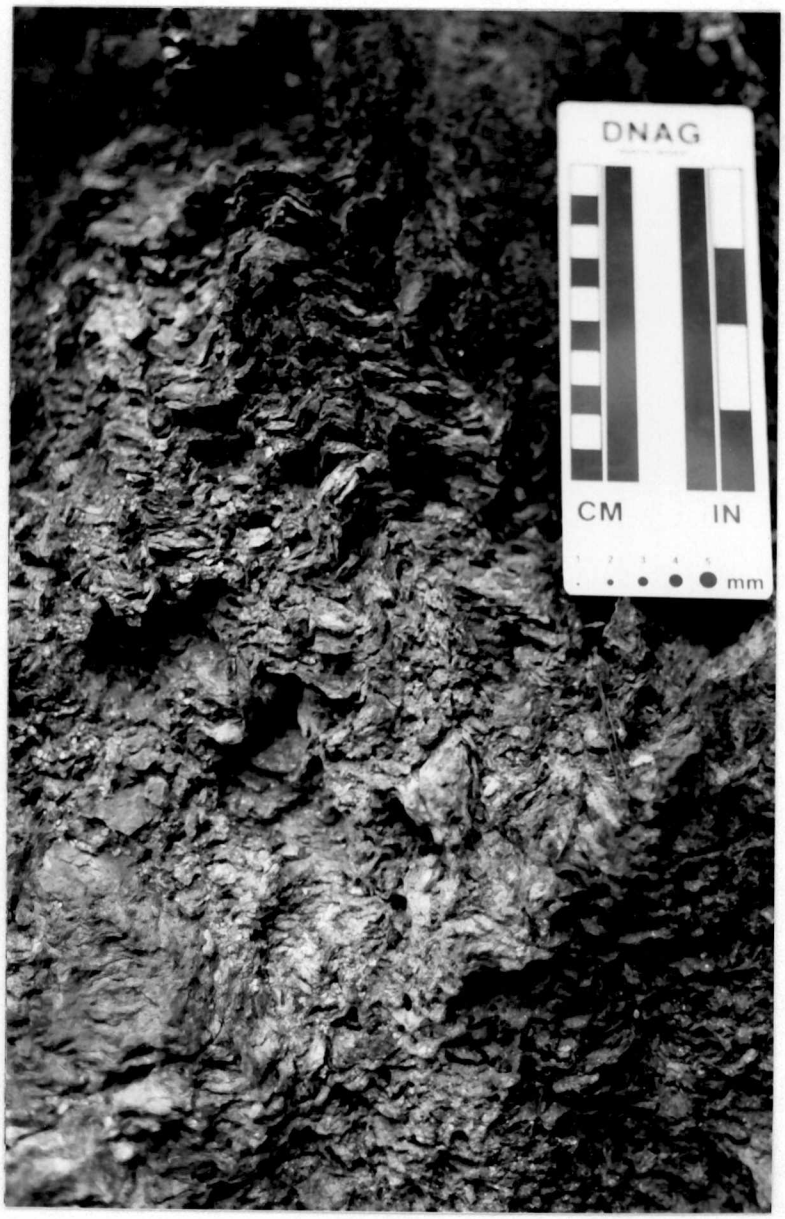


Figure 6. Outcrop photograph showing crenulations in the Ocoee Series near the Hayesville fault. (location J22, Plate, In Pocket)

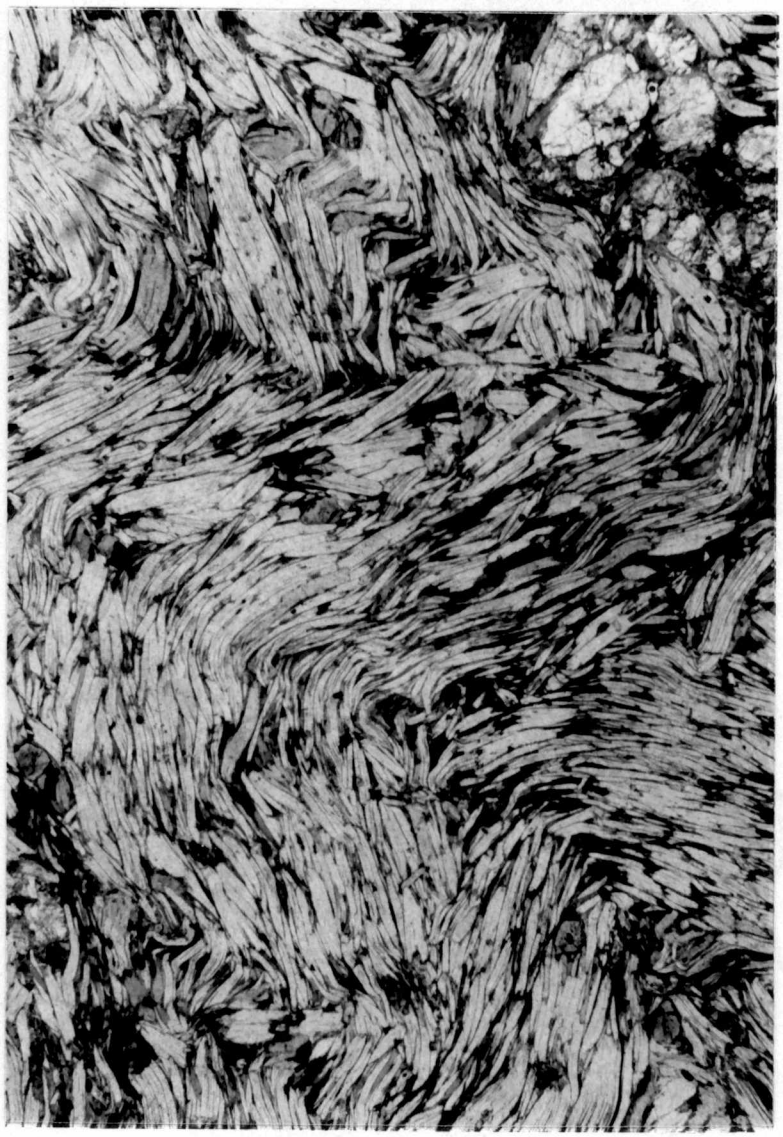


Figure 7. Photomicrograph of crenulation. Width of photograph is approximately 1.5 mm.

fault in the northern part of the study area is based on the first appearance of a very lineated sillimanite schist unit of the Otto Formation. Lineation measurements of this schist indicated a southwest plunge. Location of the fault in the southern part of the study area is more tenuous, as differences in appearance of the rocks may be due to the high metamorphic grade (near the second-sillimanite isograd). The location here is based on the truncation of petrologic units (i.e., abundance of amphibolitic pods in the Otto Formation) and on the presence of mylonite along the proposed tectonic contact.

The Soque River fault has been dated as Acadian (?) (Hopson, et al., 1989) (i.e., post-metamorphic peak). The presence of higher-grade rocks (Tallulah Falls Formation) in the hanging wall and lower-grade rocks (Otto Formation) in the footwall of the Soque River fault supports its development during post-metamorphic-peak time.

It has been suggested (Nelson, in review) that Dahlonega gold belt rocks (correlated with the Otto Formation) are laterally continuous with the Great Smoky Group; thus, Nelson suggested that the Soque River fault is the Hayesville fault.

Map-scale folds were observed within the study area on both the Hayesville and Soque River faults (Plate, In Pocket). As shown in the large-scale map of Figure 1, the Hayesville fault is also folded in the Wayah Bald area (Eckert et al., 1989), as is the Soque River fault (Hopson et al., 1989).

The sinuous trace of the early fault surfaces results from later folding.

In general, foliation, compositional layering, and fold axes in the Ocoee Series and Tallulah Falls Formation trend northeast-southwest and dip or plunge steeply to the southeast in the study area (Plate, In Pocket). Compositional layering in the Otto Formation shows greater variation in trends and dip angles. No other progressive macroscopic or mesoscopic changes in foliation trends were observed across the area.

2.2 Mesoscopic Structures and Microscopic Textures

Although projections of contacts are difficult, given the complex nature of the deformations that have affected this terrane, several generations of mesoscopic structural features are apparent. Thus, mesoscopic structures recognized in the study area provide the most valuable information for extracting and ordering the deformational events that affected the terrane. Although some outcrops of the area appear hopelessly chaotic at first glance (especially in the Otto Formation), a sequence of deformational events can be discerned and are correlated with specific deformational events given in Figure 3. The schistose, gneissic, and mylonitic fabrics from the ductile deformation of study area rocks are interpreted to be the result of compression.

As shown in Figure 3, it is proposed that S_1 is defined by an initial foliation generated during isoclinal recumbent folding designated as F_1. This early foliation is difficult

to observe given the numerous subsequent deformational events (including the formation of migmatites) which affected the terrane, and thus S_1 was not seen in the study area. Given the difficulty of observing the S_1 surface, definition of the original surface (S_0) is speculative, but contacts between amphibolitic pods and gneiss are assumed to be S_0. The S_0 surface could have been (1) compositional layering, (2) bedding (transposed by F_1), (3) tectonic contacts, or (4) intrusive sill contacts.

Hatcher and Butler (1979) observed S_1 and F_1 in the Blue Ridge with average S_1 foliation trends of east/west and dips steeply to the northeast. Where it exists in the Blue Ridge, this early foliation is defined by the parallel alignment of biotite, amphiboles, and/or platy ribbons of deformed quartz.

Folding of S_1 and the formation of an S_2 foliation is thought to be related to a second isoclinal recumbent folding event, F_2, which occurred coevally with the dominant metamorphic event during the Taconian orogeny and transposed all previous surfaces. The dominant foliation, S_2, is defined by parallel alignment of biotite, and biotite and amphibole in mafic rocks. Features associated with S_2 and F_2 are commonly the oldest mesoscopic features in the amphibolite facies because later deformational events were not so penetrative as to obliterate them. Migmatites in the study area sometimes crosscut the S_2 foliation, but are usually themselves folded and disrupted. Thus, logically the formation of migmatites is

contemporaneous with peak metamorphism. Within the granulite facies terrane, the sequence of deformational events is more difficult to discern. This may be due to the development of in situ partial melts that disrupted the foliation. The foliation in the granulite facies terrane is also considered to be S_2 because of its similar style and orientation.

The isoclinal recumbent folds of F_2 were later refolded into upright, open folds designated F_3. No overprinting foliation was developed during this deformational event. Figure 8 shows an upright F_3 fold in Tallulah Falls Formation rocks (trending N30E). Figure 9 shows the F_2 and F_3 fold generations in the Tathams Creek outcrop in the study area (location TC, Plate, In Pocket).

Structural features in the Tathams Creek outcrop are especially distinct because the exposure was recently constructed during road improvements. Although it is impossible to pick out the entire suite of deformational events in a single outcrop, four deformational events can be discerned in this outcrop (F2, F3, F4?, and F5).

This outcrop reveals complexly deformed granitic gneiss enclosing amphibolite interlayers and dikes. Lenses or pods of amphibolite often appear highly attenuated or complexly interfolded with the enclosing granitic rock (Figure 9). The amphibolite pods have a blocky appearance at one end of the outcrop but never appear to truncate the foliation. Raymond et al. (1988) designated these lenses or pods as block-in-



Figure 8. Upright F_3 fold in the Tallulah Falls Formation exposed in the town of Dillsboro. (Note geopick for scale.)

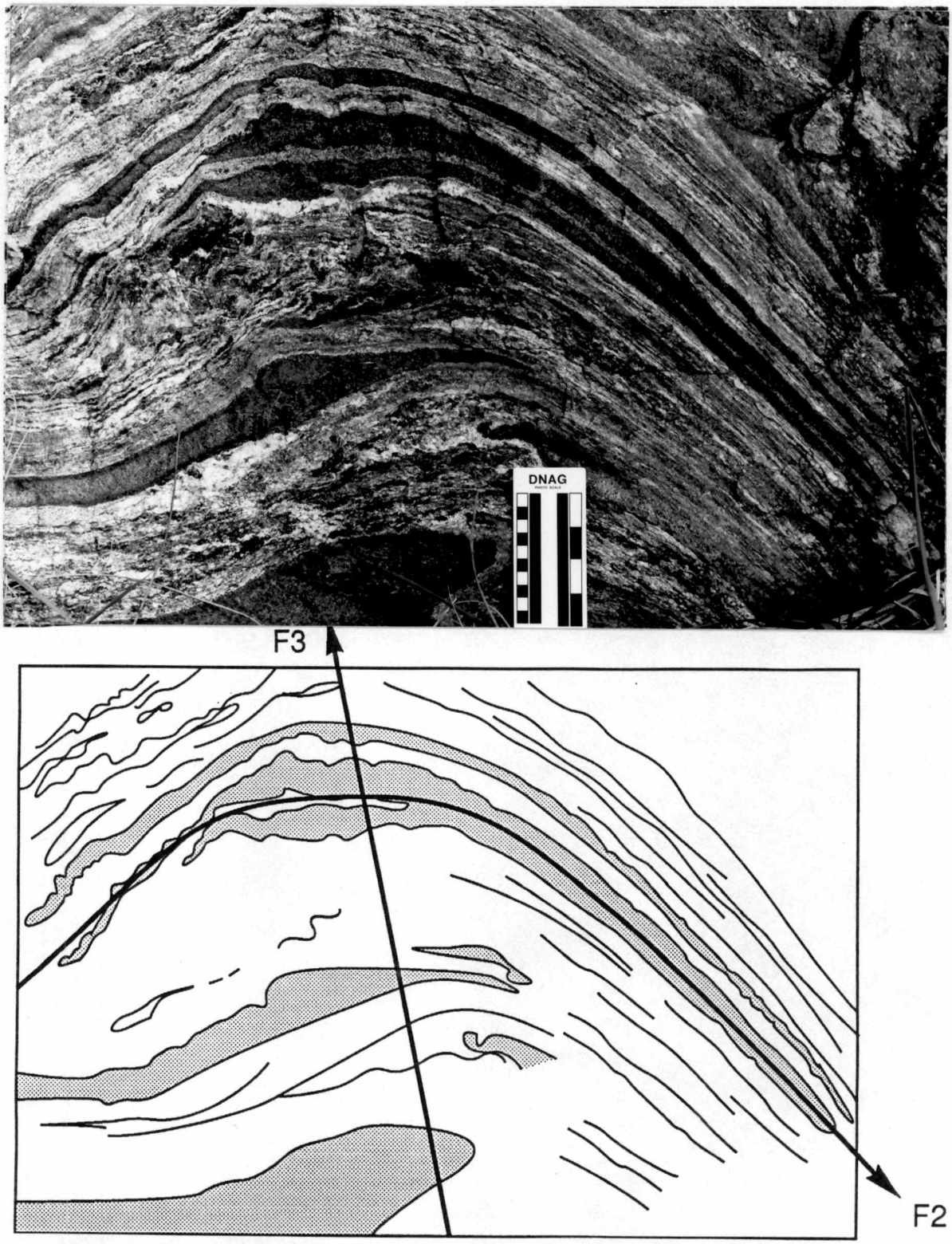


Figure 9. Fold generation in the Otto Formation at the Tathams Creek outcrop.

matrix structures and proposed that these structures were evidence for an accretionary terrane (mélange) origin of the rocks. While mesoscopic structural features may support the mélange theory, the formation of the amphibolitic pods can also be explained by the more simple mechanism of boudinage during compression or flattening normal to layering. The compressional environment began with tight folding and the eventual elimination of fold closures by attenuation and formation of discontinuities. During transposition, boudins may be formed by the segmentation of rock material that is generally more competent than the surrounding rock material (Ramsay, 1967). As the stiffer material separates, the softer material may flow in and around the boudins. At the Tathams Creek outcrop, leucocratic material was observed at the ends of the elongate boudins.

Well-developed crenulations were only observed in the schistose rocks of the Ocoee Series (see Figures 6 and 7). This late brittle deformation utilized slippage planes along the already weakened S_2 surface. These crenulations may be related to the F_4 event shown on Figure 3. All structures associated with F_1 through F_3 events are crosscut by quartz veins. Some of the quartz veins are disrupted due to tectonic flattening (F_4?) which also affects all previously described mesofabrics.

Later pegmatitic dikes (F_5?) were not disrupted by shortening and crosscut all previously discussed mesofabrics

along S_2 surfaces (Figure 10). A late, brittle deformation is locally recognized, possibly associated with F_5. This deformation has locally offset (up to 3 cm) the cross-cutting pegmatite dikes. Deformed and undeformed dikes attest to the presence of at least two generations of pegmatites.

An annealed mylonite (formed then overprinted by metamorphism) was observed just north of the Tathams Creek outcrop (location F08, Plate, In Pocket). This mylonite represents shortening with the footwall of the Soque River fault, but does not appear to juxtapose different stratigraphic sequences. Figures 11-15 show the mylonite in outcrop, hand samples, and photomicrographs. The mylonitic fabric trends N57E and is vertical. The fabric is defined by the parallel alignment of recrystallized biotite, quartz ribbons, and microshear surfaces composed of ultramylonitized material. The mylonite zone extends approximately 1000 ft and at its northern extent is in contact with an exposure of relatively undeformed granitoid. Even though the mylonite is a relatively minor feature in the study area, it suggests that shortening may have occurred within the terrane prior to metamorphism of the Otto Formation.

In thin section (Figures 13 and 15), quartz in the mylonite displays deformation by dislocation glide and creep processes. This is evident from such features as undulose extinction and the localized, <u>in situ</u> recrystallization of the grain into minute subgrains. With increasing deformation,

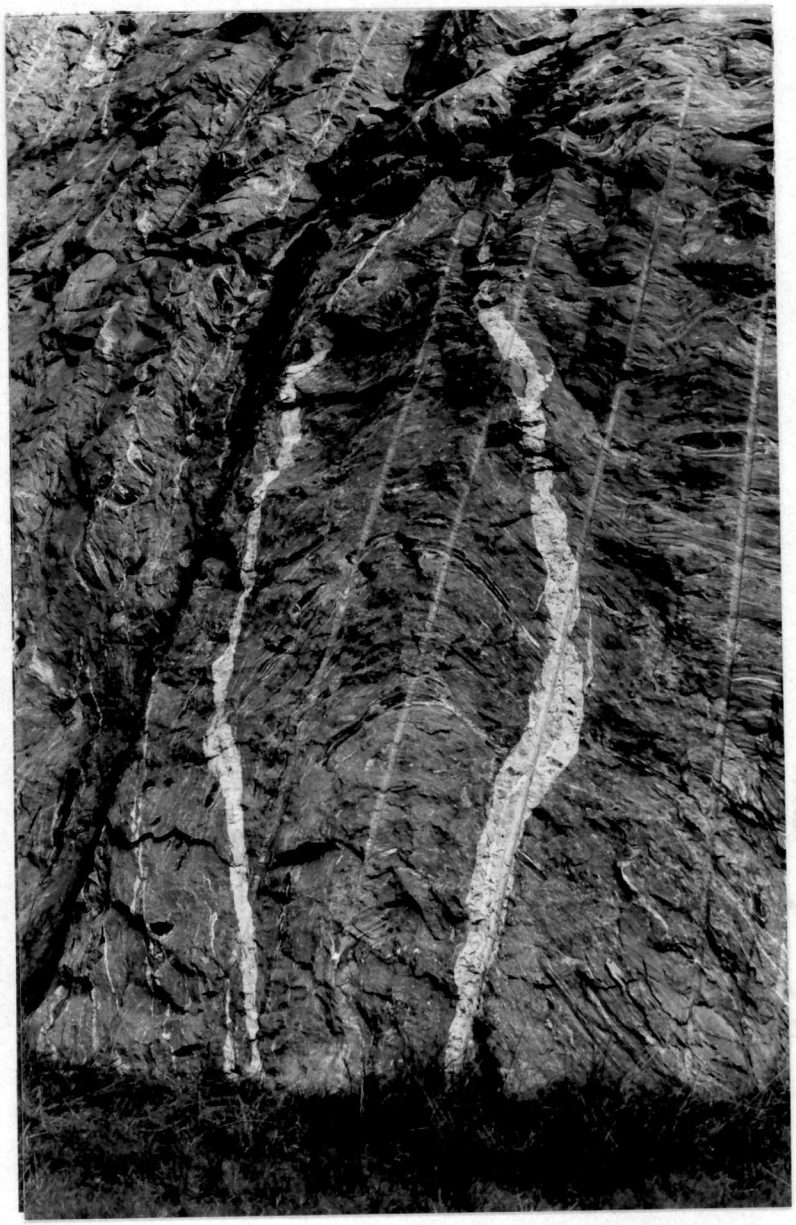


Figure 10. Undeformed pegmatite dikes. Maximum width of pegmatite dikes is approximately 9 cm.

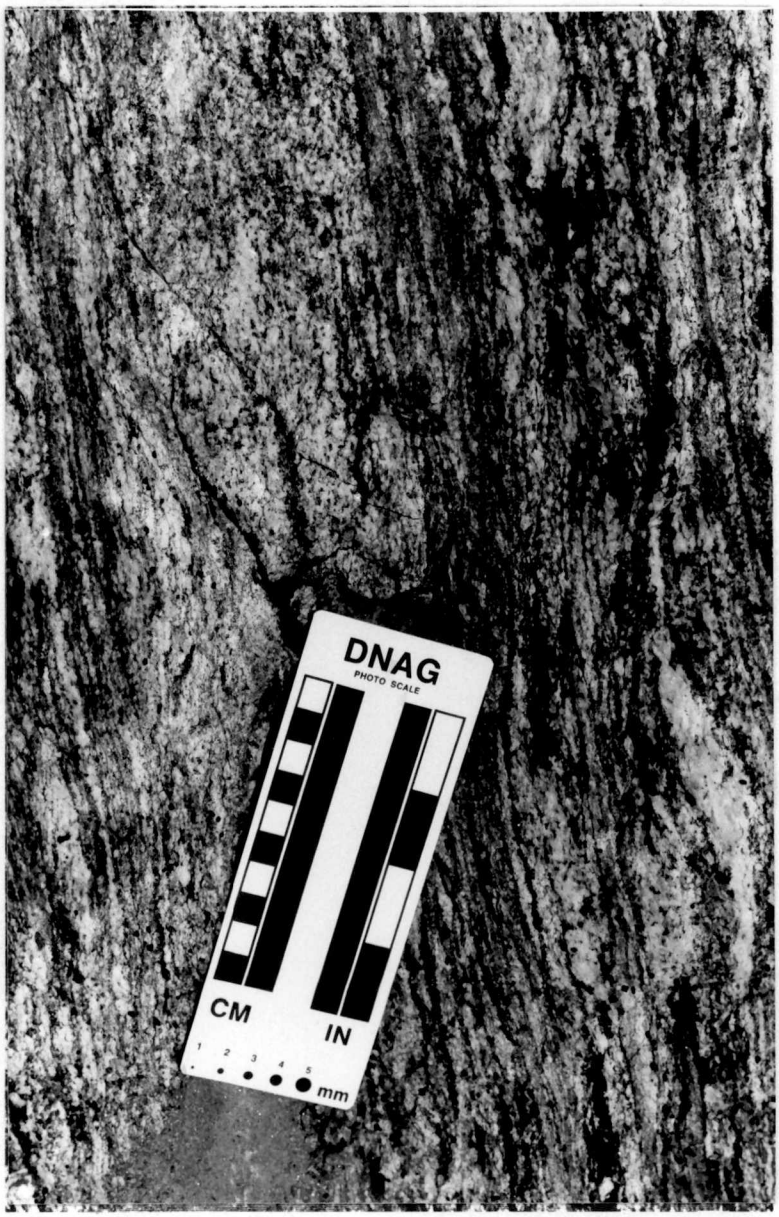


Figure 11. Mylonite in outcrop.



Figure 12. Mylonite hand sample. Note the feldspar porphyroclast.

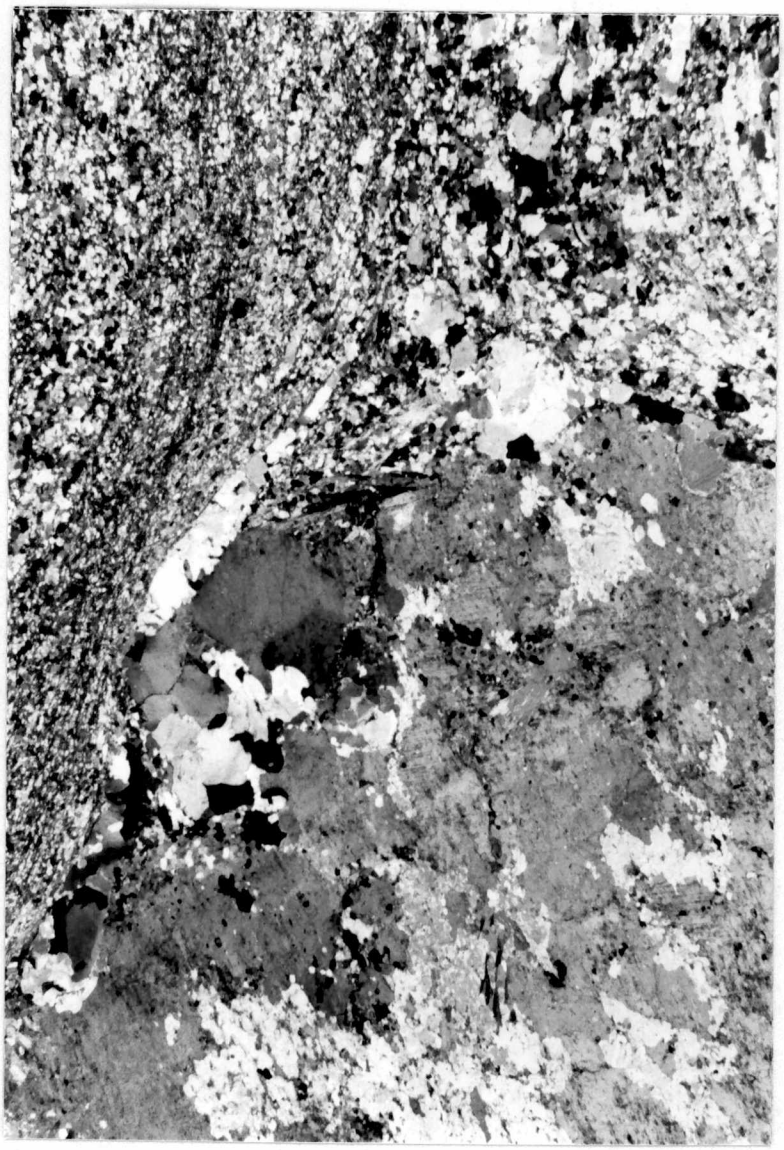


Figure 13. Mylonite photomicrograph. Width of the photograph is approximately 1.5 mm.



Figure 14. Mylonite hand sample.



Figure 15. Mylonite photomicrograph. Width of photograph is approximately 1.5 mm.

quartz grains undergo ductile deformation, forming extremely elongate, flattened undulose "ribbons" aligned parallel to the dominant shear direction (White, 1976; Simpson, 1985). In areas of especially high strain, quartz ribbons display minor recovery of dislocation creep by recrystallization (White, 1976). This is characterized by scattered patches of recrystallized subgrains. With continued strain, ribbons ultimately completely recrystallize (Figure 15). Diffusion creep may eventually lead to a polygonal mosaic of strain-free, recrystallized grains with high-angle grain boundaries (Spry, 1969; White, 1976; Bell and Etheridge, 1973). Recovery to this extent may also be caused by thermally induced "annealing" during a major metamorphic event (Tullis, 1979; Tullis et al., 1982). The annealed appearance of the mylonite constrains its formation to prior-to-peak metamorphic time.

In general, whole-rock deformation of the quartz- and feldspar-rich rocks of the terrane can be described as ductile, but the various mineral constituents of the rocks behave differently under the same deformation conditions. For example, at higher total strain, large feldspar grains deform with the strain-softening quartz. At low-grade facies conditions, feldspar grains tend to remain as large "augen", deforming by crushing and fracturing (Sibson, 1977, Simpson, 1985). At slightly higher strains but with low volumes of augen, feldspar augen rigidly rotate within the quartz, mica, and finer-grained feldspar matrix without much large-scale

intracrystalline deformation (Debat, et al., 1978; Vidal, et al., 1980). At some critical stress, an augen will "lock" in place and no longer rotate within the groundmass. Strain becomes concentrated at grain boundaries and especially at the leading and trailing edges of the augen (Figures 13 and 15) (Debat et al., 1978; Vidal et al., 1980).

As the groundmass continues to deform, the fractured or recrystallized edges of the feldspar augen are progressively dragged into the ductilely deforming groundmass, generating elongate, asymmetrical "tails" of feldspar extending parallel to the overall shear direction (Simpson and Schmid, 1983; Simpson, 1985). In the hand sample shown in Figure 12, a large feldspar augen is rounded and asymmetrically wrapped by the foliation (Figure 13).

CHAPTER 3.0

PETROGRAPHY AND MINERAL ASSEMBLAGES OF STUDY AREA LITHOLOGIES

The wide variety of rock types present in the study area provides an excellent basis to observe the metamorphic history of the terrane. Three major stratigraphic units have been identified in the study area: the Ocoee Series, the Tallulah Falls Formation, and the Otto Formation (Plate, In Pocket). Within each stratigraphic unit are distinct lithologies (i.e., schists, gneisses, and amphibolites) which will be described according to mesoscopic and microscopic observations.

Pegmatite dikes are common within all units of the field area and are a late feature, as they cross-cut all previous foliations and structures (F_1, F_2, and F_3) with a range in strike of N20E to N78E. These dikes contain plagioclase + quartz + biotite + muscovite + K-feldspar. Also, all stratigraphic units exhibit some retrograde reactions (i.e., replacement of garnet by chlorite and/or biotite in fracture fillings and of feldspar and aluminum silicate with sericite); however, the retrograde reactions were incomplete.

As suggested by Compton (1962), major minerals are listed in order of increasing abundance; thus, the most abundant mineral is placed nearest the rock name. Mineral names in parentheses in the text are not present in all rocks of a unit, but are common.

3.1 Ocoee Series/Great Smoky Group

The Ocoee Series comprises a sequence of impure to pure, west- to northeast-derived terrigenous clastics which typically occur in multiple graded sequences (McLaughlin and Hathaway, 1973). The Ocoee Series represents deposition in extensional basins that were later compressed and overthrust during early Paleozoic orogenic events (Rast and Kohles, 1986). Rocks of the Ocoee Series rest unconformably upon Grenville (1.0-1.2 Ga) basement and are probably late Proterozoic (Hatcher, 1979).

As shown on the Plate (In Pocket), the Ocoee Series is truncated by the Hayesville Fault in the northern end of the study area and is in tectonic contact with the Tallulah Falls Formation. Thus, this fault separates the rift-drift facies of the Ocoee Series from deeper water (i.e., ocean floor, continental slope-and-rise) metasedimentary rocks and associated mafic and ultramafic rocks.

The Ocoee rocks in the study area are tentatively correlated with the Copperhill Formation (the lowest formation of the Ocoee Series) as originally defined by Hurst (1955) and modified by Hernon (1967). This correlation (rather than correlation with the overlying Wehutty Formation of the Ocoee Group) is based on the absence of metaconglomerate and graphitic schist in the sequence in the study area.

Two lithologies of this formation are observed in the study area: muscovite - biotite schist and metagraywacke,

with plagioclase, quartz, muscovite, and biotite as ubiquitous minerals in the lithologies. The two lithologies are in repetitive stratigraphic contact in the study area, as a result of cyclic deposition or of isoclinal folding. The contacts are sharp, occurring with a width of approximately 25 cm and are easily observed along roadcuts between the towns of Wilmont and Dillsboro. The interlayering of the lithologies on the mesoscopic scale may represent primary bedding. This compositional layering has a range in strike of N46E to N30E and dips of 65SE to 30SE.

The metagraywacke (Figure 16) is composed mainly of quartz and feldspar with subsidiary biotite and muscovite, and the dark gray color might indicate a protolith of deep-water turbidite. This lithology is fine- to medium-grained, massive, with equidimensional grains. Some graded bedding (from coarse to fine metagraywacke) may be preserved in compositional layering, but metamorphism (amphibolite facies) and complicated tectonics (polyphase deformation) hinder exact definition of sedimentary structures.

The typical mineral association is (microcline) - (muscovite) - biotite - calcic plagioclase - quartz. The biotite is sometimes green in polarized light. This suggests a high ferric iron content relative to titanium (Deer et al., 1966). Garnet is rare in the metagraywacke.

The muscovite-biotite schist (see Figure 4a and Figure 17) has a light gray (silver) color and sometimes contains a



Figure 16. Photomicrograph of Copperhill Formation metagraywacke showing typical mosaic of quartz, plagioclase, and biotite. Width of photograph is approximately .5 mm.



Figure 17. Photomicrograph of Copperhill Formation schist. Width of photograph is approximately 1.5 mm.

yellow-sulfidic material. The biotite and muscovite are consistently aligned with, and help define, the dominant foliation. The mica grains are often kinked and display ragged grain boundaries. The dominant association is (kyanite/fibrolitic sillimanite) - garnet - quartz - plagioclase - biotite - muscovite schist. The garnets usually contain inclusions which sometimes preserve a fine-grained foliation that parallels the matrix foliation; however, in some cases the garnet has been rotated with respect to the matrix foliation. Some garnets are wrapped by the foliation and others crosscut the foliation, suggesting two periods of garnet formation. The presence of staurolite and kyanite in mylonitic rocks such as sample K04F are interpreted to be the result of retrograde reactions. Fibrolitic sillimanite occurs along muscovite/plagioclase grain boundaries, commonly with anhedral poikioblastic kyanite.

Both lithologies exhibit deformed textures associated with movement along the Hayesville fault. The schist lithology preserves the best mylonitic textures (see Figures 4b and 5); however, both the schist and metagraywacke are isoclinally folded.

3.2 Tallulah Falls Formation

The Tallulah Falls Formation consists of a sequence of biotite gneiss (metagraywacke), pelitic schist, and mafic rocks in a medium- to high-grade, migmatitic, polydeformed terrane which unconformably overlies basement (Hatcher 1971b,

1973, 1976, 1977, 1979, and 1980). Correlation of the rocks in the study area (bounded by the Hayesville and Soque River Faults) with the Tallulah Falls Formation is based on similarities to descriptions of Tallulah Falls Formation rocks and associations in the references mentioned above. Along-strike proximity to rocks designated as Tallulah Falls in the Franklin quadrangle (Kittleson, 1988) to the south, and mapping to the north-northeast in the Sylva North and Sylva South quadrangles (M. Quinn, pers. comm.) confirms the correlation.

Hatcher (1971) identified four members in this formation: (1) graywacke-schist, (2) graywacke-schist amphibolite, (3) quartzite-schist, and (4) garnet-aluminous-schist. The major rock types identified in the study area are biotite semi-schist and garnet-biotite gneiss (Figures 18-23) (both thought to be variations in Hatcher's graywacke-schist member). The most abundant rock type is a medium- to coarse-grained biotite - plagioclase - quartz gneiss which frequently contains garnet and sometimes kyanite or sillimanite. The amphibolite-bearing member becomes more common in the southern part of the study area.

Gneissic rocks are generally light gray to dark gray and commonly exhibit a pinstripe appearance due to interlayering (isoclinal folding) of quartz-feldspar and micas on the scale of 0.5 to 1.0 cm (Figures 18 and 20). These rocks have well-developed foliations defined by biotite and other platy

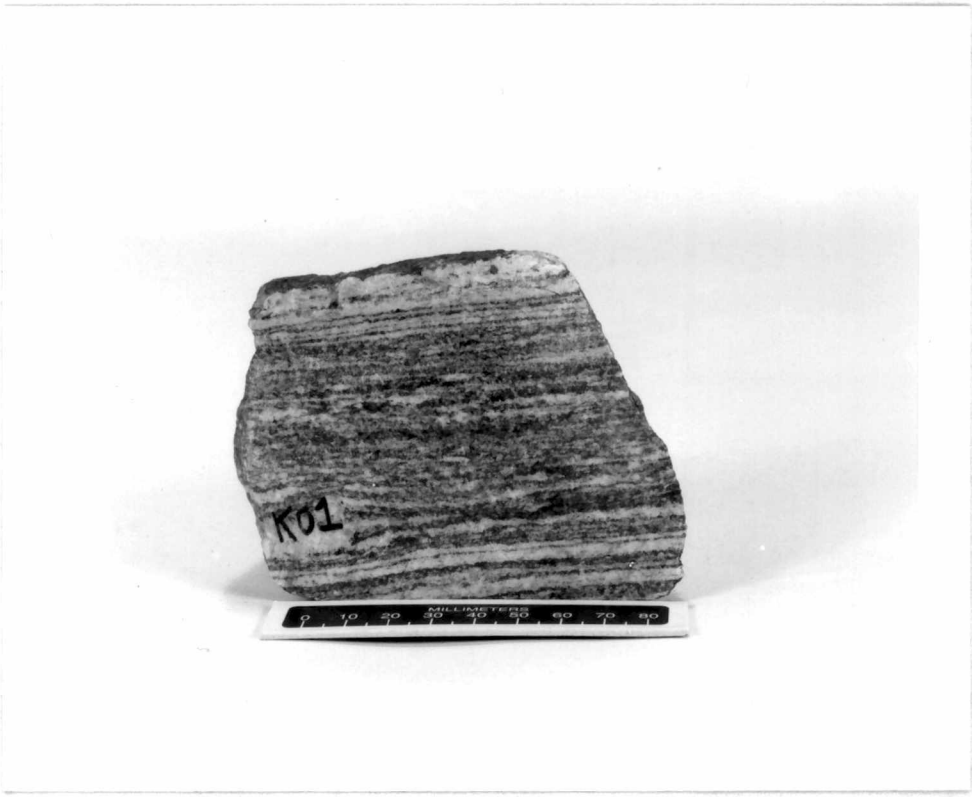


Figure 18. Tallulah Falls Formation sample from northern end of the study area.

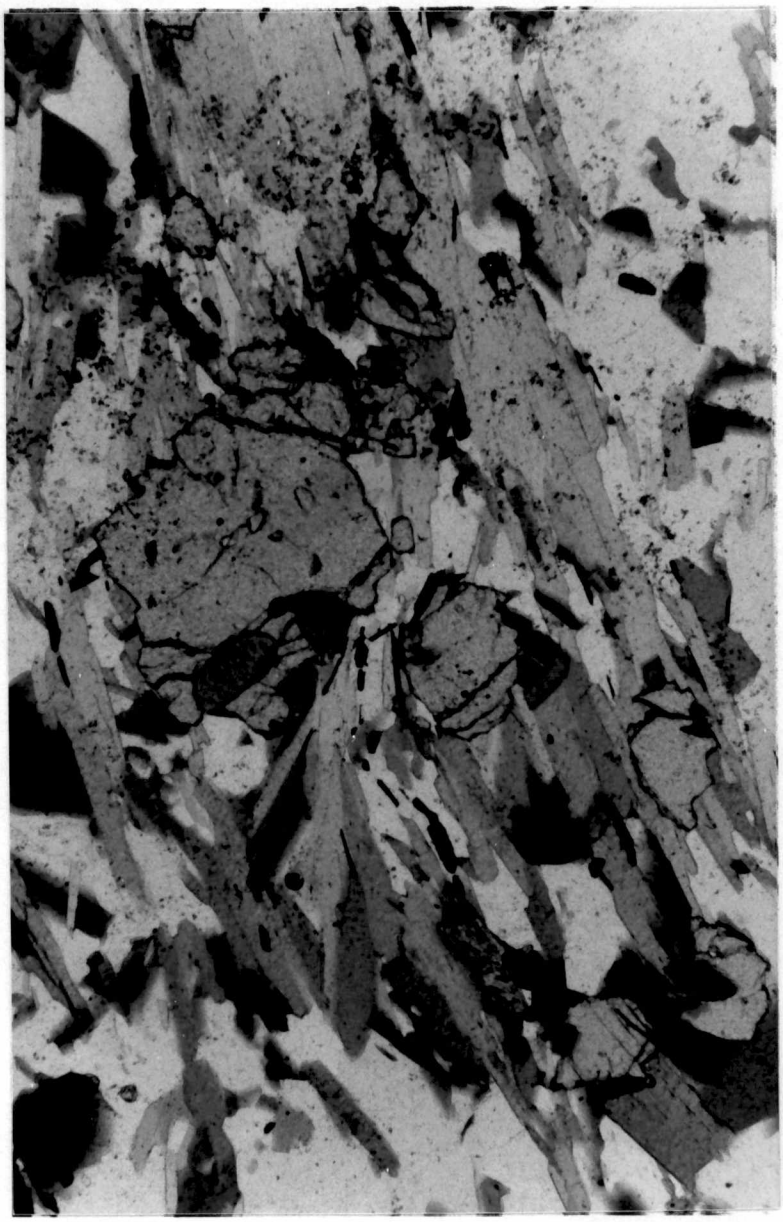


Figure 19. Photomicrograph of the Tallulah Falls Formation. Width of photograph is approximately 1.5 mm.



Figure 20. Tallulah Falls Formation biotite gneiss from the southern part of the study area. Note the partial melt bleb.



Figure 21. Photomicrograph of partial melt bleb (bottom half). Width of photograph is approximately 1.5 mm.



Figure 22. Tallulah Falls Formation biotite gneiss showing increased grain size.



Figure 23. Photomicrograph of Tallulah Falls Formation biotite gneiss under granulite facies. Width of photograph is approximately 0.75 mm.

minerals. The more felsic gneisses are commonly massive with poorly developed foliations. The garnets contain inclusions, with poikioblastic cores and the clean rims.

Eckert (1984) plotted Tallulah Falls rocks on a QFM plot and found that they fall with the area designated as graywacke by Pettijohn (1944) and Hadley and Goldsmith (1963) as modified by Ausburn (1983). These results support the interpretation of this biotite gneiss sequence as one dominated by metagraywacke.

Excellent exposure in a roadcut in the town of Dillsboro displays the Tallulah Falls Formation under amphibolite facies conditions. Here locally intensely foliated garnet-biotite gneiss is cross-cut by ptygmatic veins which are themselves disrupted and folded. This suggests that the ptygmatic veins developed during waning stages of movement along the foliation planes. Kyanite is the highest-grade mineral present in the rocks from this outcrop.

In the southern part of the study area, Tallulah Falls Formation rocks lie across the amphibolite - granulite facies transition. In the higher-grade terrane (near Franklin), garnet-biotite gneiss is again the dominant rock type with subordinate amphibolite, although sillimanite has replaced kyanite as the dominant aluminum silicate and feldspar-quartz segregations (partial melts?) sometimes disrupt the compositional layering (Figure 20). Perthitic K-feldspar is also more common in the high-grade rocks.

Quartz-feldspar segregations commonly have garnet and biotite-rich rims and are non-foliated. The quartz-feldspar segregations are interpreted to represent in situ partial melts (leucosome) and the garnet-biotite rims are thought to be restites (melanosome) (Mehnert, 1968, Ashworth, 1986). The quartz-feldspar segregations occur as pods and lenses discordant to the foliation and as discontinuous layers parallel to the foliation.

Rocks in the vicinity of location A33A (Plate, In Pocket) are the first rocks observed in the study area to have no primary muscovite and abundant sillimanite and K-feldspar (Figure 22). This sample also shows increased grain size. Thus, the northern extent of the second sillimanite isograd (i.e., the thermal core) is well constrained approximately 5 kilometers northeast of the town of Franklin. The common high-grade assemblage is (K-feldspar)-garnet - biotite - plagioclase - quartz - sillimanite.

A mafic rock collected at the southwesternmost extent of the study area reveals the coexistence of orthopyroxene and clinopyroxene, which defines the hypersthene zone of the granulite facies, but this sample was float collected from a landfill. Thus, the location of this isograd is probably nearby but cannot be located without mapping. The other minerals in the mafic assemblage are garnet, biotite, hornblende, quartz, plagioclase, and sphene.

Up gradient of the second sillimanite isograd,

sillimanite occurs in two habits. Fibrolitic sillimanite is preserved as inclusions in garnet and defines a relict foliation at an angle to the dominant foliation. Large sillimanite lathes also occur in the matrix (Figure 23).

3.3 Otto Formation

The stratigraphic unit shown in the footwall of the Soque River fault (Plate, In Pocket) is correlated with the Otto Formation, a feldspathic metasandstone interlayered with aluminous schist (Hatcher, 1988). This unit, to the southeast of Franklin is called the Dahlonega Gold belt assemblage and Helen Group and includes amphibolite facies assemblages that are also abundant in the study area. The correlation is thus based on similarities with previous descriptions and with previous work to the south (Kittleson, 1988) and with mapping in progress to the north-northeast (along strike) in the Sylva North and Sylva South quadrangles (M. Quinn, pers. comm.).

This unit in the study area is comprised of intensely foliated schistose layers (Figures 24-28) with discontinuous pods and lens of hornblende amphibolite which extend parallel to the dominant foliation. The pods never truncated foliation, and thus are interpreted to have a pre-metamorphic origin. The common assemblage in the amphibolitic rocks is (garnet) - quartz - biotite - plagioclase - hornblende, with subordinate amounts of rutile and sphene. Where the amphibolitic occur as float in weathered outcrops, a thick orange weathered rim was observed.



Figure 24. Otto Formation at the Tathams Creek location. Note the interlayered relationship of gneiss and amphibolite.



Figure 25. Photomicrograph of Otto Formation gneiss. Width of photograph is approximately 0.5 mm.



Figure 26. Otto Formation gneiss and amphibolite in upright F_3 fold.



Figure 27. Photomicrograph of Otto Formation showing an amphibolite fold nose. Width of photograph is approximately 1.5 mm.



Figure 28. Photomicrograph of the aluminous schist member of the Otto Formation. Euhedral staurolite grain is in the center of the photograph. Width of photograph is approximately 0.5 mm.

Raymond et al. (1988) included this area in their Cullowhee terrane and proposed that the amphibolitic pods in the unit were evidence of a mélange origin for the rocks. Identification of the migmatitic structures found in these rocks can be found in Raymond et al. (1988).

A very lineated garnet-sillimanite schist member of the Otto Formation aided in identifying the trace of the Soque River Fault in the northern part of the study area. The absence of amphibolic pods and associated migmatitic structures in the overlying Tallulah Falls Formation confirmed the placement of the fault trace in both the northern and southern sections of the study area. The development of migmatite is interpreted to be related to partial melting (anatexis) of the unit during peak metamorphism.

The common assemblage in rocks of pelitic composition is (kyanite) - (staurolite) - (sillimanite) - garnet - biotite - muscovite - plagioclase - quartz. The sillimanite occurred in two habits. The more felsic rocks contain biotite + plagioclase + quartz +/- garnet. Staurolite was observed in this study as euhedral grains in thin section in rocks from locations UG, TC, and D21A (Plate, In Pocket) (Figure 28). Work in the Dahlonega Gold Belt (Albino, in review) has suggested that the rocks of the Otto Formation were retrograded to staurolite during cooling since relict sillimanite was observed. However, there is no textural evidence in the study area rocks to support the formation of

staurolite by a retrograde reaction. Retrograde reactions were seen in the Otto Formation as rounded blebs of biotite in a pseudomorphic replacement of garnet. Rocks of the Otto Formation did not reach granulite facies conditions, thus, a prograde reaction for the formation of staurolite is a more probable explanation.

3.4 Mineral Chemistry

3.4.1 Pelitic rocks

Analyzed mineral assemblages in pelitic rocks of the three stratigraphic units are presented in the Appendix (Tables A.1-A.5).

Biotite is ubiquitous throughout the study area. In the Copperhill Formation, the biotite is sometimes green in polarized light. This suggests a high ferric iron content relative to titanium (Deer et al., 1966). Biotite grains contain minor amounts of Na and rarely Ca. Muscovite is also present in all three stratigraphic units, but is absent in the high-grade rocks of the Tallulah Falls Formation.

Plagioclase analyses from all three stratigraphic units plot in the upper andesine range. Lack of a trend in plagioclase compositions across the study area might suggest that metamorphic grade does not vary much, but because there are other indicators of changing grade, this probably means that Ca/(Ca+Na) is controlled by bulk composition rather than metamorphic grade in these rocks. Albite and complex (polysynthetic) twinning are common in plagioclase. In

addition, myrmekitic plagioclase was observed in the high-grade terrane.

Aluminosilicate polymorphs occur in these rocks in the form of kyanite and sillimanite. Sillimanite is usually fibrolitic in the Copperhill Formation and the low-grade rocks of the Tallulah Falls Formation. Fibrolitic sillimanite as inclusions in garnet and euhedral lathes of sillimanite are present in the high-grade rocks of the Tallulah Falls Formation. Both kyanite and sillimanite are present in the sillimanite schist lithology of the Otto Formation. Other minerals in this lithology (i.e., staurolite) confirm that this lithology is in disequilibrium.

Staurolite was analyzed in two samples from the Otto Formation. Grains range from euhedral in the sillimanite schist lithology to very irregular grain boundaries (suggesting instability) in the remainder of the low-grade Otto Formation. Small percentages of Zn are present but are generally less than .30 weight percent. TiO_2 and MnO are present only in minor quantities. This may be due to the ubiquitous presence of biotite which would act as sink for these elements.

All analyzed garnets are generally stoichiometric $(Fe,Mg,Ca,Mn)_3Al_2Si_3O_{12}$. Garnets range from euhedral and free of inclusions to heavily embayed and inclusion-rich. In the Copperhill metagraywacke, garnets are rare; however, they are common in the interlayered schist. Garnets are abundant in

the Tallulah Falls and Otto Formations and increase in size with metamorphic grade. Compositional zonation (from core to rim) was observed along the almandine-pyrope solid solution. In general, the almandine component increased in garnet rims with corresponding decreases in spessartine, grossular, and pyrope components (Figure 29). Anomalous trends were observed in a sample from the Otto Formation and one from the Tallulah Falls Formation. Sample K01 (Figure 29a) showed increasing spessartine content in garnet rims vs. cores. This could be an indication of a graywacke protolith, since spessartine is observed in metamorphosed graywacke type sediments (Deer et al., 1966). Trends in the Otto Formation and the high-grade Tallulah Falls Formation are comparable to those observed by Kittleson (1988) just to the south of the study area.

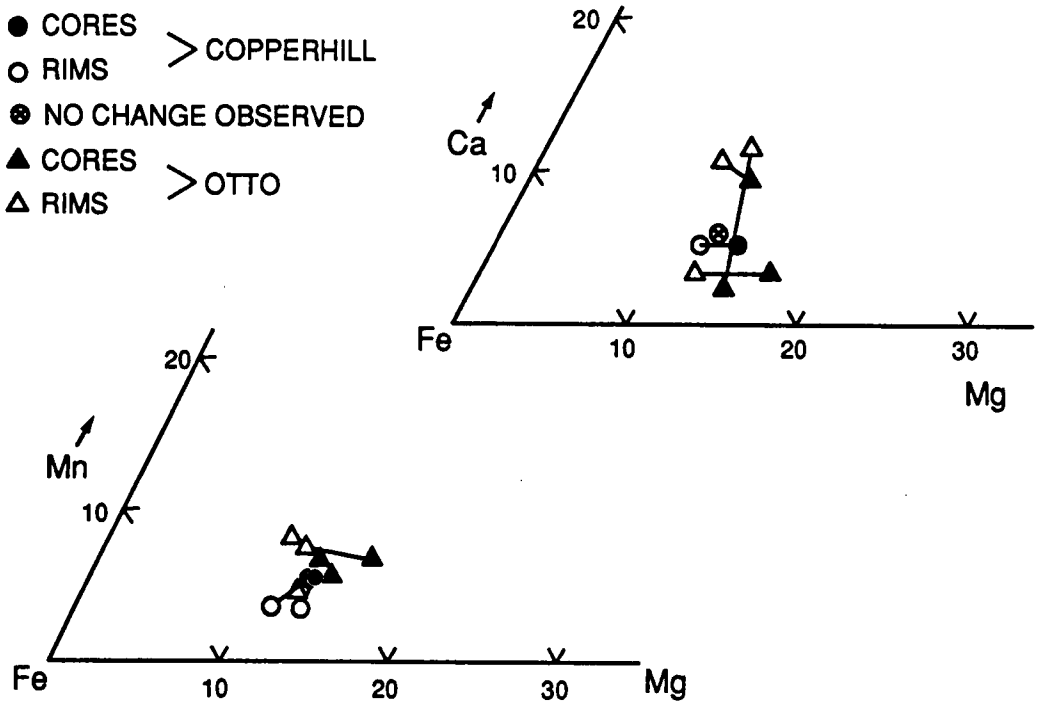
3.4.2 Amphibolitic rocks

Analyzed mineral assemblages in amphibolitic rocks of the Otto and Tallulah Falls Formation are presented in the Appendix (Tables A.6-A.8).

Hornblende is the predominant mineral in the amphibolites occurring as euhedral lathes or, alteratively, anhedral with a sponge-like appearance. Euhedral grains, along with biotite, define the foliation. Light green pleochroic anhedral hornblende is also commonly observed surrounding garnet.

Garnets range up to 1 cm in size and contain numerous inclusions. Garnets are almandine-grossular-pyrope solid

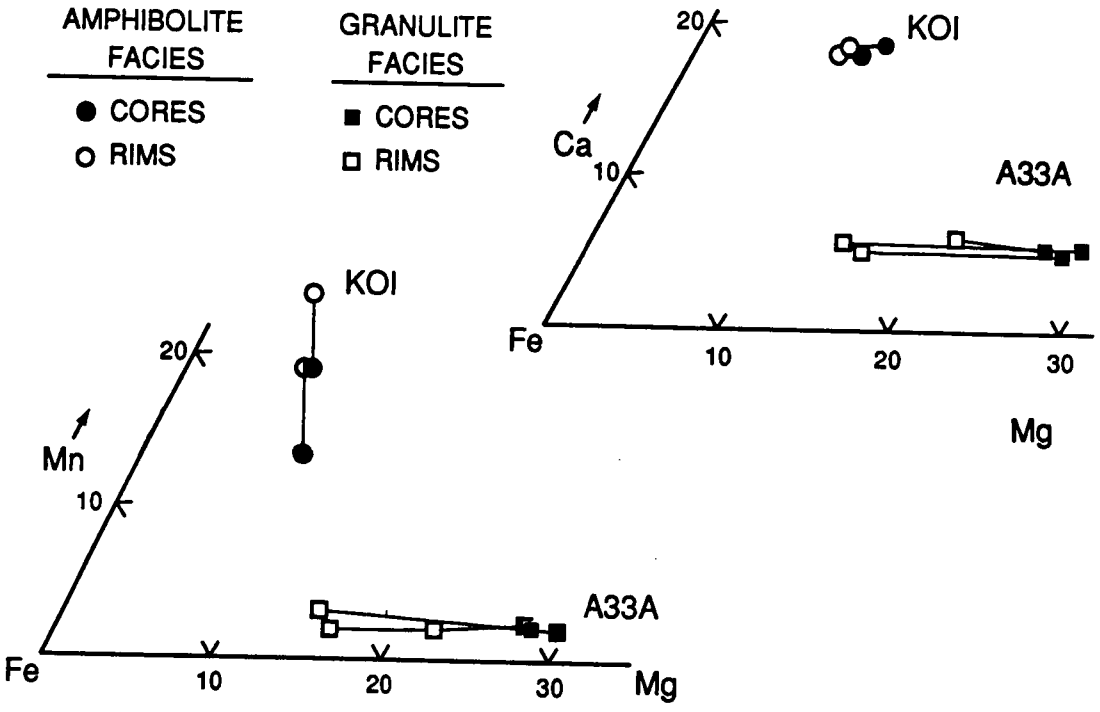
Figure 29. Garnet composition. Ternary diagrams (Mn-Fe-Mg and Ca-Fe-Mg) of coexisting core and rim garnet compositions. Closed symbols represent core compositions, open symbols represent rim compositions.



a. Copperhill and Otto Formations

(continued)

Figure 29. (continued)



b. Tallulah Falls Formation

solutions, with a minor spessartine component.

Plagioclase content varies a great deal and the amount designates either a plagioclase-hornblende amphibolite or a hornblende-plagioclase gneiss. Plagioclase compositions plot between the andesine and labradorite ranges. Anorthite content is lowest in sample CL where the plagioclase coexists with clinopyroxene.

At high-grades clinopyroxene reacts to form orthopyroxene and Ca-rich plagioclase (Deer et al., 1966). Orthopyroxene was only observed in one sample from the southwestern boundary of the study area. In this sample both orthopyroxene and clinopyroxene displayed a granular habit.

CHAPTER 4.0

REACTIONS AND CONDITIONS OF METAMORPHISM

4.1 Isograds and Metamorphic Reactions

Index minerals in the pelitic rocks of the stratigraphic units in the vicinity of the study area include sillimanite and perthitic K-feldspar. Orthopyroxene is considered an index mineral in the amphibolitic rocks. The locations of these index minerals in the vicinity of the study area indicate that isograds are elongate along strike in the field area and represent progressive metamorphism from the sillimanite zone of the amphibolite facies to the hornblende granulite facies.

The trace of the first-sillimanite isograd (based on the first appearance of fibrolitic sillimanite) lies northwest of the field area (Carpenter, 1970; Hadley and Nelson, 1971); thus, Ocoee rocks in the northern part of the study area are in the sillimanite zone of the amphibolite facies. Sillimanite sometimes occurs along muscovite-plagioclase grain boundaries, commonly with anhedral kyanite in the Copperhill schist, suggesting disequilibrium, retrogression, or coexisting equilibrium of kyanite and sillimanite.

The trace of the second-sillimanite isograd (based on the transition from muscovite and quartz assemblages to K-feldspar and sillimanite assemblages) is drawn as the elliptical end of the granulite thermal core in the southern end of the study

area (approximately 5 km northeast of Franklin) with the elongate limbs of the ellipse trending to the southwest (Plate, In Pocket). Kittleson (1988) mapped this transition a few kilometers west of Franklin; thus, the thermal core lies west of Franklin. The transition from muscovite-bearing assemblages to K-feldspar-bearing assemblages is sharp, and outcrop locations give enough control to confirm the abrupt but continuous transition. Observation of this transition coincides with the development of in situ partial melts (local segregations of leucocratic material of granitic composition formed by anatexis). The formation of the high-grade assemblage and the partial melts probably developed by the following reaction (source: Thompson and Tracy, 1979):

muscovite + albite + quartz = aluminosilicate + K-feldspar + melt.

Alternative water-producing reactions would have resulted in more complete retrograde reactions during cooling than are observed (Kittleson, 1988). Kittleson's fluid inclusion work confirmed the lack of H_2O in the system.

As shown in Figure 20, the partial melts form as small (approximately 5 cm elongate) blebs elongated parallel to the schistosity. The melts appear to have segregated locally from the host rock over a distance of centimeters.

The trace of the hypersthene isograd (based on the transition from garnet and hornblende assemblages to garnet, orthopyroxene, clinopyroxene, and hornblende assemblages in amphibolitic rocks) is assumed to lie near the extreme

southern end of the study area. The scope of the study area did not extend far enough into the thermal core to provide good control on the placement of this isograd; however, float blocks of amphibolite with the clinopyroxene and orthopyroxene assemblage were observed at the extreme southwestern end of the study area. This reaction is basically driven by the dehydration of hornblende and is proposed to be:

hornblende + quartz = orthopyroxene + clinopyroxene + plagioclase + water

The increase in the amount of garnet in the high-grade amphibolitic rocks also suggests that the following reactions may have occurred:

tremolite + anorthite = garnet + diopside + quartz + water

tremolite + anorthite = orthopyroxene + clinopyroxene + garnet + quartz + water

Another possible explanation for the increase in garnet is that partial melting left garnet as a refractory residue. Additional information on the placement of the hypersthene isograd west of Franklin can be found in Kittleson (1988).

4.2 Compositional Diagrams and Projections

AFM diagrams (after Thompson, 1957) are used here to represent mineral assemblages, assuming the presence of quartz. These diagrams allow representation of all the major components of common metamorphic rocks in a single diagram and allow the recognition of disequilibrium assemblages by the presence of crossing tie-lines.

AFM diagrams for metamorphic facies interpreted to be present in the study area are presented in Figure 30. Figure 30a shows a projection from muscovite for the amphibolite facies rocks (first-sillimanite zone). Projection from K-feldspar is utilized for the granulite facies rocks (second-sillimanite zone) (Figure 30b). This change in projection results in biotite compositions plotting within the AFM triangle in the projection from K-feldspar.

Regular partitioning of Fe and Mg is observed except for those rocks which contain staurolite (dashed lines on Figure 30a). The addition of staurolite results in a four-phase region defined by staurolite, sillimanite/kyanite, garnet, and biotite in the Otto Formation. As described in Chapter 3, staurolite occurs as euhedral grains in the Otto Formation. The presence of euhedral staurolite probably represents a prograde reaction where staurolite is formed by the breakdown of garnet. A previous study in the Otto Formation further to the south suggested that the staurolite was formed from a retrograde reaction because of the coexistence of staurolite with relict sillimanite. Textural evidence from the study area does not support the formation of staurolite by a retrograde reaction. Alternatively, I propose that because staurolite is stable in the sillimanite field, the presence of staurolite is the result of a prograde reaction.

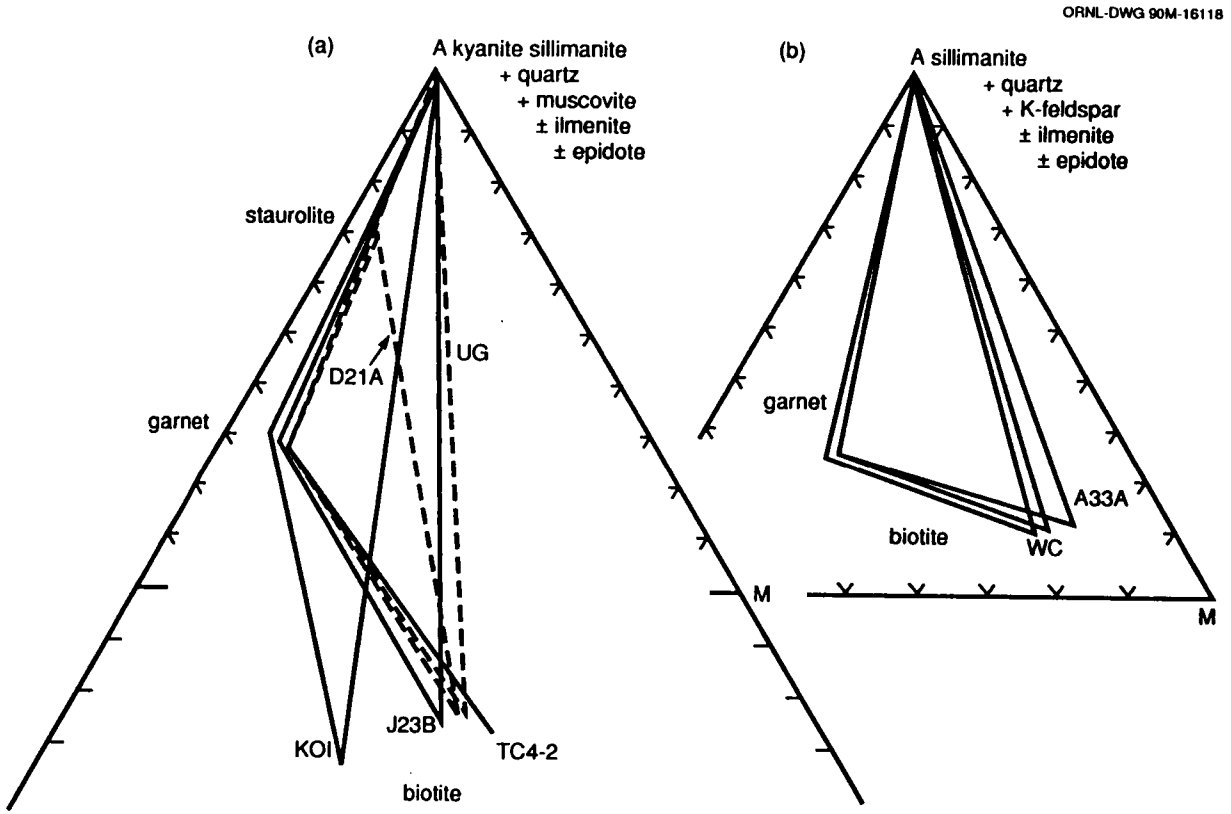


Figure 30. AFM projections (after Thompson, 1957) for pelitic rocks. (a) Projection from muscovite for the amphibolite facies assemblages. Dashed lines indicate those assemblages that cross-cut the other tie-lines and are presumed to be disequilibrium assemblages. (b) Projection from K-feldspar for granulite facies assemblages.

Assemblages represented here support metamorphism of rocks in the study area at medium to high temperatures and medium pressure.

4.3 Pressure and Temperature Indicators

4.3.1 Pressure and Temperature from Reaction Relationships

Constraints on the pressure and temperature of the study area rocks can be made based on reactions that have been studied experimentally. For example, for pelitic rocks, certain assemblages can be constrained by utilizing the maximum temperature stability limits of kyanite, staurolite, and muscovite, and the minimum temperature limit of sillimanite (Figure 31). The aluminosilicate triple point shown on Figure 31 was determined experimentally by Holdaway (1971). The limit of staurolite stability was determined by Ganguly (1972), and the limit of muscovite stability was determined by Kerrick (1972). Work by Thompson (1976) has established the upper limit of cordierite, which constrains the minimum pressure (approximately 5.75 kbar) across the study area because cordierite was not observed in any assemblage.

The most common assemblage, garnet + biotite + sillimanite + muscovite + quartz, which is found in the Copperhill Formation and the low-grade rocks of the Tallulah Falls Formation, is constrained by the lower temperature limit of sillimanite, and the maximum temperature limits of staurolite and muscovite stability in the presence of quartz.

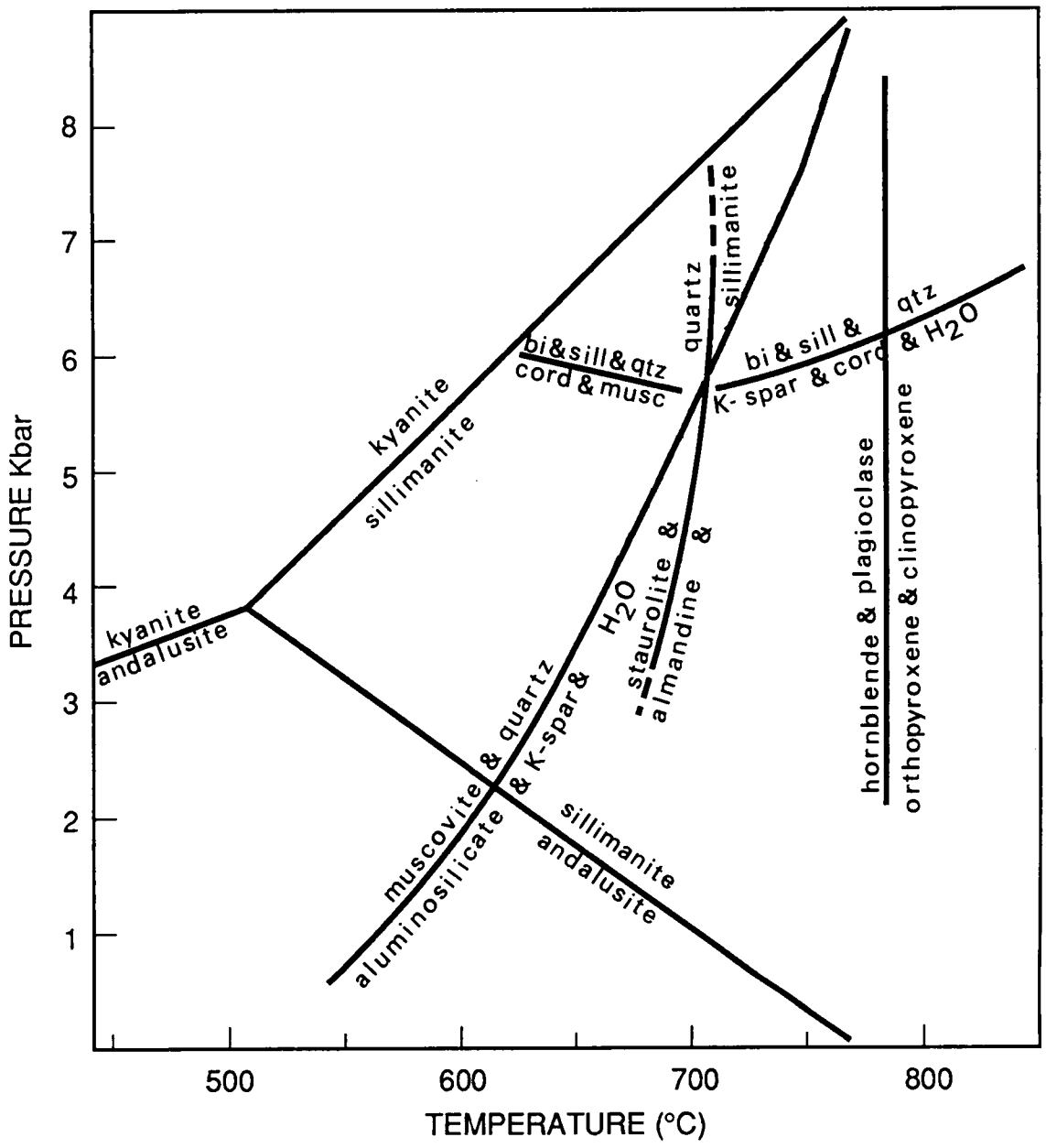


Figure 31. Relevant mineral equilibria for the pressure and temperature conditions of medium- to high-grade metamorphism for study area assemblages.

The intersection of muscovite and staurolite stability curves place lower temperature and pressure limits of approximately 675 °C and 5.75 kbar on this assemblage. The intersection of sillimanite and muscovite stability curves places upper temperature and pressure limits of 8.0 kbar and 750 °C.

The assemblage garnet + sillimanite + biotite + K-feldspar + quartz is found in high-grade pelitic rocks and the assemblage hornblende + garnet + orthopyroxene + clinopyroxene is found in high-grade amphibolitic rocks of the Tallulah Falls Formation. The intersection of cordierite and muscovite stability fields places lower pressure and temperature limits of 6.0 kbar and 700 °C. A maximum temperature of 800 °C between 6.5 and 9.75 kbar is obtained by the intersection of hornblende, cordierite, and sillimanite stability.

The constraints of pressure and temperature on these assemblages would suggest that the transition for amphibolite to granulite facies (along the muscovite breakdown reaction) occurred between 675 and 750 °C at pressures of 6.5 to 7.5 kbar.

4.3.2 Temperature Calculations from Mineral Exchange Equilibria Calculations

Mineral compositions in the pelitic rocks can be used to estimate temperature during metamorphism. For example, Fe and Mg partitioning between coexisting garnet and biotite is temperature dependent with pressure having very little effect

on the partitioning. Thus, with increasing temperature, biotite becomes more Fe-rich and garnet becomes more Mg-rich.

In order to determine temperatures which were as close to peak metamorphic conditions as possible, samples for quantitative study on the electron microprobe were chosen based on the following criteria:

1. freshness of sample: no obvious retrograde reactions or weathered samples
2. representation of study area stratigraphic units
3. relative abundance of garnet vs. biotite to minimize the effect of reequilibration

Representative microprobe analyses are presented in the Appendix.

A variety of calibrations for the garnet-biotite (Fe-Mg exchange) geothermometer have been proposed. Calculations from calibrations by Ferry and Spear (1978), Indares and Martignole (1986), Perchuk and Lavrent'eva (1983), and Ganguly and Saxena (1984) are presented in Table 1 for several coexisting garnet-biotite compositions across the study area.

Garnet core with biotite matrix (biotite not in contact with a garnet), and garnet rim with biotite in contact with a garnet were used to calculate temperature. Rim garnet and adjacent biotite gave consistently lower estimates than garnet core and biotite matrix. Therefore, garnet core-biotite matrix analyses were used as the best estimate of peak metamorphic conditions, but these must be recognized as

Table 1. Garnet-biotite temperature estimates (in °C) for both garnet core-biotite matrix and garnet rim-biotite rim associations.

Sample	Association	FS	IM	GS	PL
J23B	core-matrix	575	495	585	589
	core-matrix	566	496	583	584
	rim-rim	518	445	541	556
	rim-rim	540	474	551	569
K01	core-matrix	652	585	630	712
	core-matrix	611	553	672	609
	rim-rim	534	543	566	611
	rim-rim	550	512	575	620
WC	core-matrix	767	534	639	686
	core-matrix	775	529	646	689
	rim-rim	568	436	489	585
	rim-rim	549	428	478	575
A33A	core-matrix	1067	866	924	805
	core-matrix	1173	946	997	840
	rim-rim	724	630	668	665
	rim-rim	659	529	643	633
UG	core-matrix	554	510	543	577
	core-matrix	563	523	563	583
	rim-rim	456	418	470	519
	rim-rim	478	438	503	533
TC4-2	core-matrix	597	549	598	601
	core-matrix	552	509	566	576
	rim-rim	507	503	548	552
	rim-rim	501	493	556	546
D21A	core-matrix	512	453	518	553
	core-matrix	536	469	531	567
	rim-rim	482	443	499	535
	rim-rim	487	443	497	538

(FS = Ferry and Spear), (IM = Indares and Martignole), (GS = Ganguly and Saxena), (PL = Perchuk and Lavrent'eva)

minimum estimates because of the possible reequilibration of garnet and biotite during cooling.

Ferry and Spear's (1978) experimentally calibrated thermometer is based upon experiments in systems with Fe/Fe+Mg held at approximately 0.9. The Ferry and Spear calibration has two additional screens, Ca + Mn in garnet < 0.2 and $Ti+Al_{IV}$ in biotite < 0.15. Using Ferry and Spear as a experimental base, Indares and Martignole (1985) utilized data from natural assemblages to derive a thermometer which attempts to take into account the effect of these dilutents. Ganguly and Saxena (1984) used ideal mixing in biotite and nonideal mixing in garnet to fit a thermodynamic model to the experimental data of Ferry and Spear. Mimicking the original work by Ferry and Spear, Perchuk and Lavrent'eva (1983) experimentally calibrated their thermometer in systems that averaged around 0.6 Fe/Fe+Mg.

Almost identical trends were observed regardless of the calibration used. The absolute temperatures do, however, show large variation. In almost every comparison, the Indares and Martignole thermometer resulted in the lowest temperature. Temperatures from this calibration do not correlate well with the experimental mineral equilibria curves shown on Figure 31 and the observed study area assemblages. Thus, the calculations using this calibration may not represent the metamorphic conditions of the study area.

The three remaining calibrations showed similar results for assemblages from the Copperhill and Otto Formations, with the Perchuk-Lavrent'eva calibration giving the highest temperatures. The temperatures calculated using the Perchuk-Lavrent'eva model best agree with the mineral equilibria reactions and the first-sillimanite zone assemblages observed in the study area.

Temperatures calculated for the higher-grade assemblages (i.e., Tallulah Falls Formation) showed the greatest disparity among the models with a range of over 200 °C separating the Ferry and Spear result from the Perchuk and Lavrent'eva result in sample A33A. Because $Ti+Al_{VI}$ often exceeds the screen of 0.15 in the higher-grade assemblages, the Ferry and Spear model is probably not appropriate for these rocks.

Chipera and Perkins (1988) found that geothermometers based solely on ln K_d (i.e., Perchuk and Lavrent'eva, 1983) were found to give more precise results than the calibrations that attempt to incorporate non-Fe-Mg components (i.e., Indares and Martignole, 1985). In a study in a Canadian granulite terrane they concluded that the Perchuk and Lavrent'eva thermometer yielded the most precise and accurate results, estimating metamorphic temperature trends to $\pm$ 30 °C. Thus, using the Perchuk and Lavrent'eva calibration, temperature under amphibolite facies metamorphic conditions is estimated to have ranged from 550 - 600 °C. Temperatures in the granulite facies are bracketed between 670-800 °C.

Mineral assemblages containing garnet, aluminosilicate, plagioclase, and quartz can be used to estimate pressure (Ghent, 1976). The calibration used has a reported error of ± 0.5 kbar. In the amphibolite facies terrane this calculation gives a value of 5.5 kbar, and within the granulite facies terrane values ranged from 6.5 to 7.5 kbar.

Results of the geothermometry and geobarometry are summarized in Figure 32. Comparison of the results indicates that the southern part of the study area (the granulite terrane) was at a higher temperature and pressure than the amphibolite terrane.

A gradual transition from amphibolite to granulite facies conditions is not apparent in the study area. The lack of transition possibly suggests that a tectonic contact separates rocks metamorphosed to amphibolite facies from granulite facies rocks. Because granulite terranes of Grenville age have been found in other parts of the Blue Ridge (Gulley, 1985), it is possible that the thermal core near Franklin also represents Precambrian metamorphism. However, Absher and McSween (1985) found that the structural history of the granulite terrane is more similar to the lower-grade Paleozoic rocks than the Grenville-age rocks exposed elsewhere. In addition, in later studies across the amphibolite-granulite facies transition to the south both Kittleson (1988) and Eckert et al. (1989) found a gradual change in metamorphic grade and found no evidence supporting a tectonic contact

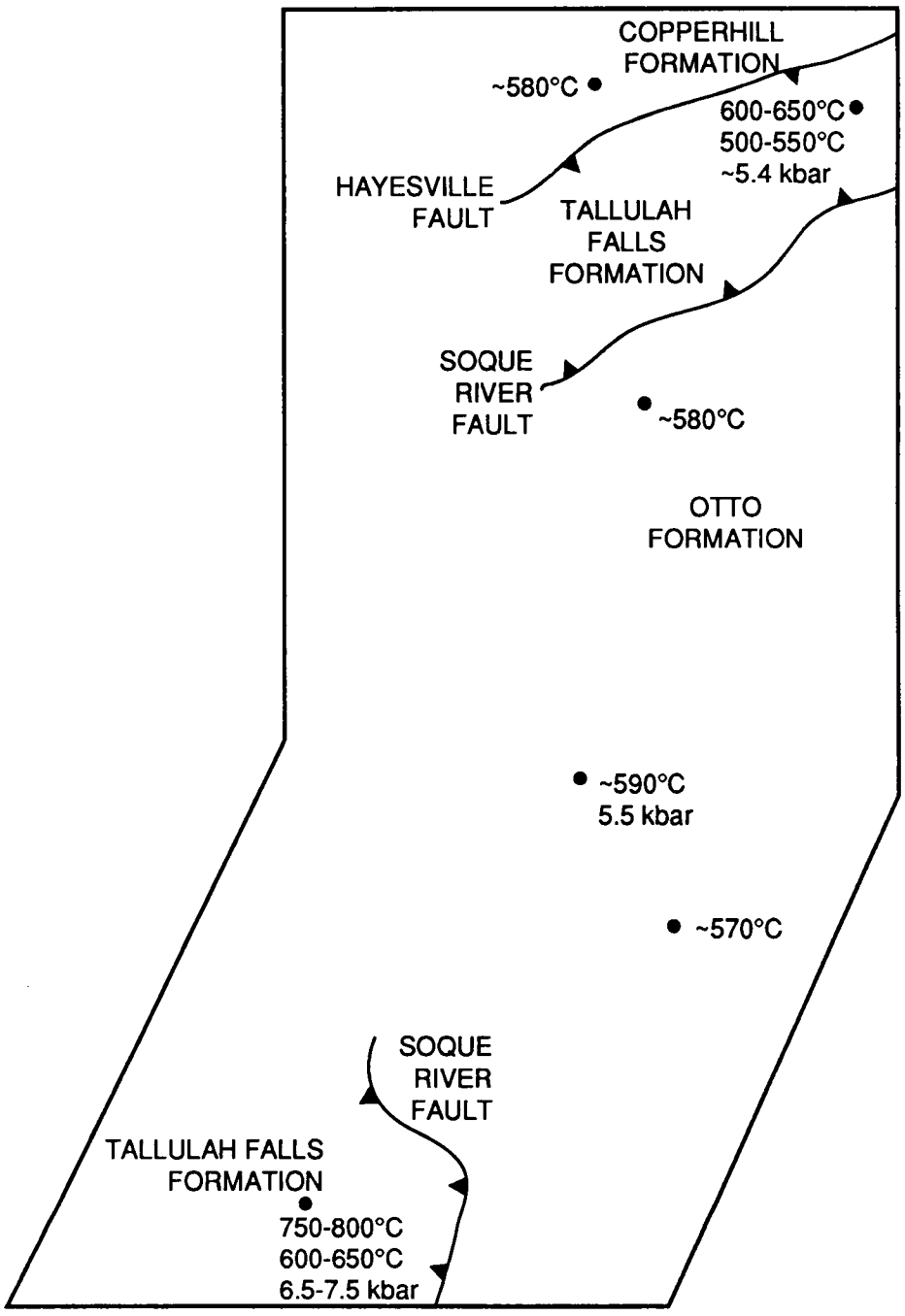


Figure 32. Estimated temperatures using mineral exchange equilibria equations. The top number or range represents temperatures calculated using data from garnet cores and matrix biotite. The middle number or range represents temperatures calculated using data from garnet rims and adjacent biotite. The bottom number or range represents pressures.

between the amphibolite terrane and the granulite terrane. Therefore, even though a gradual transition from amphibolite to granulite facies is not apparent in the study area and the Soque River fault appears to juxtapose amphibolite facies rocks and granulite facies rocks in the southern part of the study area, this apparent juxtaposition was not observed further to the south (Kittleson, 1988) nor in the northern part of the study area and is, thus, locally coincidental.

Metamorphism due to continental thickening can result from overthrusting during increased tectonic activity. This mechanism is the most feasible explanation for the metamorphism observed in the study area because of the presence of a syn-metamorphic thrust fault and the absence of pre- to syn-metamorphic magmatic intrusions (i.e., additional heat sources). The increased tectonic activity would correspond with the Taconian orogeny, supposedly a time of plate collision along the North American craton (Hatcher, 1978).

CHAPTER 5.0

CONCLUSIONS

(1) A contact between the Copperhill Formation (Ocoee Series) and the Tallulah Falls Formation can be delineated in the Whittier and Greens Creek quadrangles. This contact is designated as the Hayesville fault and appears to telescope terranes of different metamorphic history.

(2) A contact in the northern (Greens Creek quadrangle) and southern (Corbin Knob quadrangle) ends of the study area is designated as a continuation of the Soque River fault, which places the higher grade Tallulah Falls Formation over the lower grade Otto Formation. The fault disrupts metamorphic grade, and is thus a post-metamorphic fault.

(3) An along-strike Barrovian metamorphic sequence observed along the northern edge of the granulite facies terrane is the same as the sequence described for the western (Eckert et al., 1989) and eastern (Kittleson, 1988) edges of the terrane. Although narrow in width, the study area provides good control on delineation of the northern extent of the second-sillimanite isograd at the transition from the amphibolite to granulite facies. Furthermore, structural history and style in the study area are similar to the previously developed deformation schemes.

(4) Temperatures and pressures are estimated to have been 550-600 °C and 5.5 kbar in the amphibolite facies, and 670-800

°C and 6.5-7.5 kbar in the granulite facies based on mineral exchange equilibria and on geothermometry and geobarometry cation exchange equations.

(5) Continental thickening (resulting from an overthrusting mechanism at a compressional plate boundary) with a corresponding increase in temperature appears to have been the primary mechanism by which this terrane was formed.

LIST OF REFERENCES

Absher, B.S., 1984, Petrogenesis of granulite facies rocks at Winding Stair Gap, North Carolina Blue Ridge (M.S. thesis): University of Tennessee, Knoxville, 131 p.

Absher, B.S., and McSween, Jr., H.Y., 1985, Granulites at Winding Stair Gap, North Carolina: The thermal axis of Paleozoic metamorphism in the southern Appalachians: Geological Society of America Bulletin, v. 96, p. 588-599.

Albee, A.L., and Ray, L., 1970, Correction factors for electron probe microanalysis of silicates, oxides, carbonates, phosphates, and sulfates: Analytical Chemistry, v. 42, p. 1408-1414.

Ashworth, J.R., 1986, Myrmekite replacing albite in prograde metamorphism: American Mineralogist, v. 71, p. 895-899.

Ausburn, M.P., 1983, Stratigraphy, structure and petrology of the northern half of the Topton Quadrangle, North Carolina (M.S. thesis): Florida State University, 197 p.

Bell, T. and Etheridge, M., 1976 The deformation and recrystallization of quartz in a mylonite zone, Central Australia: Tectonophysics, v. 32, p. 235-267.

Bence, A.E., and Albee, A.L., 1968, Empirical correction factors for the electron microanalysis of silicates and oxides: Journal of Geology, v. 76, p. 382-403.

Bohlen, S.R., 1983, Retrograde P-T paths for granulites: EOS (American Geophysical Union Transactions), v. 64, p. 878.

Butler, J.R., 1972, Age of Paleozoic Regional Metamorphism in the Carolinas, Georgia, and Tennessee Southern Appalachians: American Journal of Science, v. 272, p. 319-333.

Butler, J.R., 1973, Paleozoic Deformation and Metamorphism in part of the Blue Ridge Thrust Sheet, North Carolina: American Journal of Science, Cooper v. 273-A, p. 72-88.

Butler , J.R., and Fullagar, P.D., 1982, Timing of orogenic events in the Carolinas: Geological Society of America Abstracts with Programs, v. 14, p. 8.

Carpenter, R.H., 1970, Metamorphic History of the Blue Ridge Province of Tennessee and North Carolina: Geological Society of America Bulletin, v. 81, p. 749-762.

Chipera, S.J. and Perkins, D., 1988, Evaluation of biotite-garnet geothermometers: application to the English River subprovince, Ontario: Contributions to Mineral Petrology, v. 98, p. 40-48.

Cook, F.A., Albaugh, D.S., Brown, L.D., Kaufman, S., and Oliver, J.E., 1979, Thin-skinned tectonics in the crystalline southern Appalachians; COCORP seismic-reflection profiling of the Blue Ridge and Piedmont: Geology, v. 7, p. 563-568.

Compton, R.R., 1962, Manual of Field Geology, John Wiley and Sons, Inc., New York.

Dallmeyer, R.D., 1975, Incremental $^{40}Ar/^{39}Ar$ Ages of Biotite and Hornblende from Retrograded Basement Gneisses of the Southern Blue Ridge: Their Bearing on the Age of Paleozoic Metamorphism: American Journal of Science, v. 275, p. 444-460.

Debat, P., Soula, J., Kubin, L., and Vidal, L., 1978, Optical studies of natural deformation microstructures in feldspars (gneisses and pegmatites from Occitanie, southern France): Lithos, v. 11, p. 133-146.

Deer, W.A., Howie, R.A., and Zussman, J., 1966, An Introduction to the Rock-Forming Minerals, Longman Group Limited, Essex, England.

Eckert, J.O., Jr., 1984, Stratigraphy, structure, and metamorphism in the east half of the Wayah Bald quadrangle, North Carolina: Key to Paleozoic granulite facies metamorphism in the southern Appalachians (M.S. thesis): University of South Carolina, Columbia, 411 p.

Eckert, J.O., Jr., 1988, Petrology and tectonic implications of the transition from the staurolite-kyanite zone to the Wayah granulite-facies metamorphic core, south west North Carolina Blue Ridge: Including quantitative analysis of mineral homogeneity (Ph.D. dissertation): Texas A&M University, College Station, 337 p.

Eckert, Jr., J.O., Hatcher, Jr., R.D., and Mohr, D.W., 1989, The Wayah granulite-facies metamorphic core, southwestern North Carolina: High-grade culmination of Taconic metamorphism in the southern Blue Ridge: Geological Society of America Bulletin, v. 101, p. 1434-1447.

Ferry, J.M., and Spear, F.S., 1978, Experimental calibration of the partitioning of Fe and Mg between biotite and garnet: Contributions to Mineralogy and Petrology, v. 66, p. 113-117.

Force, E.R., 1976, Metamorphic source rocks of titanium placer deposits - a geochemical cycle: U.S. Geological Survey Professional Paper 959-B, 13 p.

Ganguly, J., 1972, Staurolite stability and related paragenesis theory, experiments, and applications: Journal of Petrology, v. 13, p. 335-365.

Ganguly, J. and Saxena, S.K., 1984, Mixing properties of aluminosilicate garnets: constraints from natural and experimental data, and applications to geothermometry: American Mineralogist, v. 69, p. 88-97.

Gillon, K.A., 1982, Stratigraphy, structural, and metamorphic geology of portions of the Cowrock and Helen, Georgia 7.5 minute quadrangles (M.S. thesis): University of Georgia, Athens, 236 p.

Glover, III, L., Speer, J.A., Russell, G.S., and Farrar, S.S., 1983, Ages of regional metamorphism and ductile deformation in the central and southern Appalachians: Lithos, v. 16, p. 223-245.

Gulley, G., 1985, A Proterozoic granulite-facies terrane on Roan mountain western Blue Ridge belt, North Carolina-Tennessee: Geological Society of America Bulletin, v. 96, p. 1428-1439.

Hadley, J.B., and Goldsmith, R., 1963, Geology of the eastern Great Smoky Mountains, North Carolina and Tennessee: U.S. Geological Survey Professional Paper 349-B, 118 p.

Hadley, J.B., and Nelson, A.E., 1971, Geologic map of the Knoxville quadrangle, North Carolina, Tennessee, and South Carolina: U.S. Geological Survey Map, Miscellaneous Geologic Investigations, 1-654, scale 1/250,000.

Hatcher, R.D., Jr., 1971b, Geology of Rabun and Habersham Counties, Georgia: A reconnaissance study: Georgia Geological Survey Bulletin 83, 43 p.

Hatcher, R.D., Jr., 1972, Developmental model for the southern Appalachians: Geological Society of America Bulletin, v. 83, p. 2735-2760.

Hatcher, R.D., Jr., 1973, Basement versus cover rocks in the Blue Ridge of Northeast Georgia, Northwestern South Carolina, and adjacent North Carolina: American Journal of Science, v. 273, p. 671-685.

Hatcher, R.D., Jr., 1976, Carolina Geological Society Field Trip Guidebook: Introduction to the Geology of the Eastern Blue Ridge of the Carolinas and nearby Georgia.

Hatcher, R.D., Jr., 1977, Macroscopic polyphase folding illustrated by the Toxaway dome, eastern Blue Ridge, South Carolina-North Carolina: Geological Society of America Bulletin, v. 88, p. 1678-1688.

Hatcher, R.D., Jr., 1978, Tectonics of the Western Piedmont and Blue Ridge, Southern Appalachians: Review and Speculation: American Journal of Science, v. 278, p. 276-304.

Hatcher, R.D., Jr., and Zeitz, I., 1979, Tectonic Implications of Regional Aeromagnetic and Gravity Data from the Southern Appalachians: The Caledonides in the USA.: IGCP, p. 235-240.

Hatcher, R.D., Jr., 1979, Geologic Synthesis of the Tennessee-Carolinas-Northeast Georgia Southern Appalachians: The Caledonides in the U.S.A., I.G.C.P., p. 83-90.

Hatcher, R.D., Jr., and Butler, J.R., 1979, Guidebook for southern Appalachians field trip in the Carolinas, Tennessee and northeastern Georgia: International Geologic Correlation Program-Caledonide Orogen Project 27, University of North Carolina, Chapel Hill, 117 p.

Hatcher, R.D., Jr., Acker, L.L., Bryan, J.G., and Godfrey, S.C., 1979, the Hayesville thrust of the central Blue Ridge of North Carolina and nearby Georgia: A pre-metamorphic, polydeformed thrust and cryptic suture within the Blue Ridge thrust sheet: Geological Society of America Abstracts with Programs, v. 11, p. 181.

Hatcher, R.D., Jr., Butler, J.R., Fullagar, P.D., Secor, D.T., and Snoke, A.W., 1980, Geologic synthesis of the Tennessee-Carolinas, northeast Georgia southern Appalachians, in Wones, D.R., ed., The Caledonides in the USA: International Geological Correlation Program, Memoir 2, p. 83-90.

Hatcher, R.D., Jr., 1980, Timing of thrusting in the southern Appalachians, USA: model for orogeny?: J. geol. Soc. London, v. 137, p. 321-327.

Hatcher, R.D., Jr., Hooper, R.J., Petty, S.M., and Willis, J.D., 1984, Structure and chemical petrology of three southern Appalachian mafic-ultramafic complexes and their bearing upon the tectonics of emplacement and origin of Appalachian ultramafic bodies: American Journal of Science, v. 284, p. 494-506.

Hatcher, R.D., Jr., Hopson, J.L., Edelman, S.H., Liu, A., McClellan, E.A., and Stieve, A.L., 1987, Detailed geologic map of the Appalachian Ultradeep Core Hole (ADCOH) region: Structure of the southern Appalachians internides: Geological Society of America Abstracts with Programs, v. 18, p. 631.

Hatcher, R.D., Jr., 1988, Bedrock geology and regional geologic setting of Coweeta Hydrologic Laboratory in the eastern Blue Ridge, in Swank, W.T., and Crossley, D.A., Jr., eds., Ecological Studies, Volume 66: Forest Hydrology and Ecology at Coweeta: Springer-Verlag, New York, p. 81-92.

Hernon, R. M., 1967, The Wehutty Formation of North Carolina: U.S. Geological Survey Bulletin 1274-A, p. A49-A59.

Holdaway, M.J., 1971, Stability of andalusite and the aluminum silicate diagram: American Journal of Science, v. 271, p. 97-131.

Hopson, J.L., Hatcher, R.D., Jr., and Stieve, A.L., 1989, Geology of the Eastern Blue Ridge, Northeastern Georgia and the Adjacent Carolinas: Georgia Geological Society Guidebooks, v. 9, p. 1-40.

Hurst, V.J., 1955, Stratigraphy, structure and mineral resources of the Mineral Bluff quadrangle, Georgia: Georgia Geological Survey Bulletin, v. 63, 137 p.

Indares, A., and Martignole, H., 1985, Biotite-garnet geothermometry in the granulite facies: the influence of Ti and Al in biotite: American Mineralogist, v. 70, p. 272-278.

Indares, A., and Martignole, H., 1986, Biotite-garnet geothermometry in granulite facies rocks, evaluation of equilibrium criteria: Canadian Mineralogist, v. 70, p. 272-278.

Kerrick, D.M., 1972, Experimental determination of muscovite and quartz stability with $P(H_2O)<P(total)$: American Journal of Science, v. 272, p. 946-958.

Kittleson, R.C., 1988, The amphibolite-to-granulite facies transition in the Franklin and Corbin Knob Quadrangles, North Carolina Blue Ridge (M.S. thesis): University of Tennessee, Knoxville, 111 p.

Larrabee, D.M., 1966 Map showing distribution of ultramafic and intrusive mafic rocks from northern New Jersey to eastern Alabama: U.S. Geological Survey Miscellaneous Geological Investigation Map I-476, scale 1/5000,000.

Long, L.E., Kulp, J.L., and Eckelman, F.D., 1959, Chronology of major metamorphic events in the southeastern United States, American Journal of Science, v. 257, p. 585-603.

McLaughlin, R.E., and Hathaway, D.J., 1973, Fossils in the Murphy Marble: Geologic Society of America Abstracts with Programs, v. 5, no. 6, p. 418-419..

McSween, H.Y., Jr., and Hatcher, R.D., Jr., 1985, Ophiolites (?) of the southern Appalachian Blue Ridge, in Woodward, N.B., ed., Field trips in the southern Appalachians: University of Tennessee Department of Geological Sciences Studies in Geology 9, p. 144-171.

Mehnert, K.R., 1968, Migmatites and the origin of granitic rocks: Elsevier, Amsterdam, 393 p.

Nelson, A.E., 1982, Geologic map of the Tray Mountain Roadless Area, northern Georgia: U.S. Geological Survey Miscellaneous Field Studies Map MF-1347-A, scale 1/30,000.

Nelson, A.E., in review, Structure and chemistry of metasedimentary and metavolcanic rocks of the Helen terrane in the Blue Ridge structural province of northeast Georgia: Geological Society of America Special Paper.

Perchuk, L.L. and Lavrent'eva, I.V., 1983, Experimental investigation of exchange equilibria in the system cordierite-garnet-biotite: in Saxena, S.K., ed., Kinetics and equilibrium in mineral reactions: Springer, New York, p. 199-239.

Pettijohn, F.J., 1954, Classification of sandstones, Journal of Geology 62: 360-365.

Quinn, M., 1990, personal communication.

Quinn, M., (in prep.), Two Lithotectonic Boundaries in Western North Carolina: Geologic Interpretation of a Region Surrounding Sylva, Jackson County, North Carolina (M.S. thesis): University of Tennessee-Knoxville.

Ramsay, J.G., 1967, Folding and fracturing of rocks, McGraw-Hill Book Company, New York.

Rankin, D.W., 1975, The Continental Margin of Eastern North America in the Southern Appalachians: The Opening and Closing of the Proto-Atlantic Ocean: American Journal of Science, v. 275-A, p. 298-336.

Rast, N. and Kohles, K.M., 1986, The Origin of the Ocoee Supergroup: American Journal of Science, v. 286, p. 593-616.

Raymond, L.A., Yurkovich, S.P., and McKinney, M., 1988, Block-in-matrix structures in the North Carolina Blue Ridge Belt and their significance for the tectonic history of the Southern Appalachian Orogen: Geological Society of America Special Paper 228.

Shireman, J., Labotka, T., and Knapp, S., 1985, Metamorphic history of a portion of the North Carolina Blue Ridge: Geological Society of America Abstracts with Programs, v. 17, no. 2, p. 135.

Sibson, R., 1977, Fault rocks and fault mechanisms: J. Geol. Soc. London, v. 133, p. 191-213.

Simpson, C., and Schmid, S.M., 1983, An evaluation of criteria to deduce the sense of movement in sheared rocks: Geological Society of America Bulletin, v. 94, p. 1281-1288.

Simpson, C., 1985, Strain and shape-fabric variations associated with ductile shear zones: Journal of Structural Geology, v. 5, p. 61-72.

Spry, A., 1969, Metamorphic textures, Pergamon Press, New York.

Thompson, J.B., Jr., 1957, The Graphical Analysis of Mineral Assemblages in Pelitic Schists: The American Mineralogist, v. 42, p. 842-858.

Thompson, A.B., 1976, Mineral reactions in pelitic rocks: II. Calculation of some P-T-X (Fe-Mg) phase relations: American Journal of Science, v. 276, p. 425-454.

Thompson, A.B. and Tracy, R.J., 1979, Model systems for anatexis of pelitic rocks, II: Contributions to Mineralogy and Petrology, v. 63, p. 247-269.

Tullis, J.A., 1979, High Temperature Deformation of Rocks and Minerals: Reviews of Geophysics and Space Physics, v. 17, p. 1137-1154.

Tullis, J., Snoke, A., Todd, V., 1982, Penrose Conference report: significance and petrogenesis of mylonitic rocks: Geology, v. 10, p. 227-230.

Vidal, J., Kubin, L., Debat, P., and Soula, J., 1980, Deformation and dynamic recrystallization of K-feldspar augen in orthogneiss from Montagne Noire, southern France: Lithos, v. 13, p. 247-255.

White, S., 1976, The effects of strain on microstructures, fabrics and deformation mechanisms in quartzites: Phil. Trans. R. Soc., v. 283A, p. 69-86.

APPENDIX
MICROPROBE DATA

Sample numbers on this page are listed by increasing grade in stratigraphic units. See Plate, in pocket for sample locations.

Pelitic Rocks Sample Number	Stratigraphic Unit
J23B	Copperhill Formation (schist)
UG	Otto Formation (aluminous schist)
TC4-2	Otto Formation
D21A	Otto Formation
K01	Tallulah Falls Formation
WC	Tallulah Falls Formation
A33A	Tallulah Falls Formation

Amphibolite Rocks Sample Number	Stratigraphic Unit
TC	Otto Formation
CL	Otto Formation
A	Tallulah Falls Formation

Table A.1. Representative garnet analyses in pelitic rocks

Sample	K01		J23B		UG		TC4-2	
	core	rim	core	rim	core	rim	core	rim
SiO_2	36.60	36.40	36.97	36.42	36.98	36.76	37.64	37.72
Al_2O_3	21.08	21.30	21.34	21.74	21.01	20.70	20.61	19.98
FeO	33.15	31.66	35.31	35.98	35.16	35.35	33.21	33.42
MgO	2.60	1.91	3.19	3.16	3.20	2.56	3.23	2.89
MnO	3.79	5.98	2.09	1.47	3.09	3.52	2.57	2.99
CaO	3.52	3.50	1.96	2.00	1.28	1.02	3.21	3.52
TOTAL	100.74	100.75	100.86	100.77	100.72	99.91	100.47	100.52
Formula moles, based on 12 oxygens								
Si	2.95	2.94	2.96	2.92	2.97	2.99	3.01	3.03
Al	2.00	2.03	2.02	2.06	1.99	1.98	1.94	1.89
Fe	2.23	2.14	2.37	2.42	2.36	2.40	2.22	2.25
Mg	0.31	0.23	0.38	0.38	0.38	0.31	0.39	0.35
Ca	0.30	0.30	0.17	0.17	0.11	0.09	0.28	0.30
Mn	0.26	0.41	0.14	0.10	0.21	0.24	0.17	0.20
TOTAL	8.05	8.05	8.03	8.05	8.03	8.02	8.02	8.02

(continued)

Table A.1. Representative garnet analyses in pelitic rocks (continued)

Sample	D21A		WC		A33A	
	core	rim	core	rim	core	rim
SiO_2	36.63	37.69	37.14	36.55	38.10	37.26
Al_2O_3	21.13	20.84	22.39	21.80	21.63	21.37
FeO	35.96	35.47	30.59	32.22	30.12	35.66
MgO	3.41	2.94	8.16	6.98	8.34	3.96
MnO	2.32	2.12	0.57	0.70	0.50	0.80
CaO	0.96	1.43	2.09	2.01	2.02	1.90
TOTAL	100.41	100.49	100.94	100.26	100.71	100.95
Formula moles, based on 12 oxygens						
Si	2.95	3.02	2.89	2.89	2.96	2.97
Al	2.01	1.97	2.05	2.03	1.98	2.01
Fe	2.43	2.38	1.99	2.13	1.95	2.37
Mg	0.41	0.35	0.95	0.82	0.96	0.47
Ca	0.08	0.12	0.17	0.17	0.17	0.16
Mn	0.16	0.14	0.04	0.05	0.03	0.54
TOTAL	8.04	7.99	8.09	8.09	8.06	8.03

Table A.2. Representative biotite analyses in pelitic rocks

Sample	K01		J23B		UG		
	matrix	rim	matrix	rim	matrix	rim	inclusion
SiO_2	35.56	35.63	36.55	36.06	35.76	33.39	36.48
TiO_2	3.31	2.30	1.86	2.21	1.64	1.38	0.95
Al_2O_3	18.45	18.23	19.55	19.41	19.70	20.04	18.73
FeO	21.97	22.51	18.33	19.39	18.12	17.79	14.59
MnO	0.00	0.14	0.06	0.00	0.00	0.00	0.00
MgO	7.67	8.52	10.77	10.40	12.17	12.23	15.61
Na_2O	0.00	0.09	0.30	0.30	0.37	0.31	0.59
K_2O	9.71	9.84	9.54	9.60	9.58	9.73	8.59
TOTAL	96.67	97.26	96.96	97.37	97.34	94.87	95.54
Formula moles, based on 24 oxygens							
Si	5.41	5.41	5.42	5.36	5.29	5.10	5.39
Al_{IV}	2.59	2.59	2.58	2.64	2.71	2.90	2.61
Al_{VI}	0.71	0.67	0.84	0.77	0.73	0.72	0.64
Ti	0.38	0.26	0.21	0.25	0.18	0.16	0.11
Fe	2.79	2.86	2.27	2.41	2.24	2.27	1.80
Mn	0.00	0.02	0.01	0.00	0.00	0.00	0.00
Mg	1.74	1.93	2.38	2.31	2.69	2.79	3.43
Na	0.00	0.03	0.09	0.09	0.11	0.09	0.17
K	1.88	1.91	1.81	1.82	1.81	1.90	1.62
TOTAL	15.50	15.67	15.61	15.64	15.76	15.93	15.77

(continued)

Table A.2. Representative biotite analyses in pelitic rocks (continued)

Sample	TC4-2		D21A		WC		A33A	
	rim	inclusion	matrix	rim	matrix	rim	matrix	rim
SiO_2	35.80	36.18	35.96	32.87	36.67	37.51	36.71	36.57
TiO_2	1.86	2.90	1.74	1.64	4.54	3.24	1.78	2.21
Al_2O_3	17.57	17.64	19.51	20.18	17.46	18.09	18.40	19.13
FeO	20.71	16.70	18.00	18.98	13.55	12.37	13.91	18.72
MnO	0.00	0.00	0.00	0.00	0.00	0.00	0.00	0.00
MgO	10.11	12.58	11.50	11.60	12.59	15.11	14.89	10.66
Na_2O	0.00	0.21	0.42	0.50	0.00	0.00	0.00	0.00
K_2O	9.10	9.30	9.57	9.49	10.25	10.36	9.09	10.09
TOTAL	95.15	95.51	96.70	95.26	95.06	96.68	94.78	97.38
Formula moles, based on 24 oxygens								
Si	5.48	5.42	5.35	5.04	5.46	5.45	5.45	5.43
Al_{IV}	2.52	2.58	2.65	2.96	2.54	2.55	2.55	2.57
Al_{VI}	0.65	0.54	0.78	0.68	0.53	0.55	0.67	0.77
Ti	0.21	0.33	0.19	0.19	0.51	0.35	0.20	0.25
Fe	2.65	2.09	2.24	2.43	1.69	1.50	1.73	2.32
Mn	0.00	0.00	0.00	0.00	0.00	0.00	0.00	0.00
Mg	2.31	2.81	2.55	2.65	2.80	3.27	3.29	2.36
Na	0.00	0.06	0.12	0.15	0.00	0.00	0.00	0.00
K	1.78	1.78	1.82	1.85	1.95	1.92	1.72	1.91
TOTAL	15.61	15.61	15.71	15.95	15.47	15.60	15.60	15.61

Table A.3. Representative muscovite analyses in pelitic rocks

Sample	K01	J23B	UG	D21A	C16A	A33A
SiO_2	46.46	46.93	44.73	46.76	45.93	46.39
TiO2	1.71	1.27	0.46	0.38	0.23	0.52
Al_2O_3	33.64	35.46	35.94	35.38	34.64	32.29
FeO	1.89	1.25	1.46	1.79	1.89	3.71
MgO	1.00	0.85	1.03	0.57	1.16	1.12
MnO	0.01	0.03	0.00	0.00	0.00	0.00
NaO	0.28	0.83	1.05	1.90	0.00	0.00
K_2O	10.79	10.02	10.24	8.73	10.36	10.33
TOTAL	95.78	96.64	94.91	95.51	94.21	94.36
Formula moles, based on 24 oxygens						
Si	6.19	6.15	6.00	6.18	6.18	6.30
Al_{IV}	1.81	1.85	2.00	1.82	1.82	1.70
Al_{VI}	3.47	3.62	3.68	3.70	3.68	3.47
Ti	0.17	0.13	0.05	0.04	0.02	0.05
Fe	0.21	0.14	0.16	0.20	0.21	0.42
Mg	0.20	0.17	0.21	0.11	0.23	0.23
Mn	0.00	0.00	0.00	0.00	0.00	0.00
Na	0.07	0.21	0.27	0.49	0.00	0.00
K	1.83	1.67	1.75	1.47	1.78	1.79
TOTAL	13.95	13.94	14.12	14.00	13.93	13.96

Table A.4. Representative plagioclase and K-feldspar analyses in pelitic rocks

Sample	K01	J23B	TC4-2	C16A	WC		A33A
SiO_2	60.48	61.77	61.43	61.79	60.57	64.80	60.18
Al_2O_3	24.90	24.21	24.25	23.85	24.55	18.84	25.19
FeO	0.09	0.30	0.03	0.05	0.00	0.08	0.00
CaO	6.45	5.35	5.71	5.98	6.39	0.00	6.75
BaO	0.00	0.00	0.00	0.00	0.00	0.00	0.00
Na_2O	7.73	8.44	8.65	8.30	7.96	1.60	7.65
K_2O	0.12	0.11	0.13	0.11	0.20	14.76	0.27
TOTAL	99.77	100.18	100.20	100.08	99.67	100.08	100.04
Formula moles, based on 8 oxygens							
Si	2.69	2.74	2.72	2.74	2.70	2.98	2.68
Al	1.31	1.26	1.27	1.25	1.29	1.02	1.32
Ca	0.31	0.25	0.27	0.28	0.31	0.00	0.32
Ba	0.00	0.00	0.00	0.00	0.00	0.00	0.00
Na	0.67	0.72	0.74	0.71	0.69	0.14	0.66
K	0.01	0.01	0.01	0.01	0.01	0.87	0.02
Fe	0.00	0.01	0.00	0.00	0.00	0.00	0.00
TOTAL	4.99	5.00	5.02	5.00	5.00	5.01	5.00

Table A.5. Representative staurolite analyses in pelitic rocks

Sample	UG	D21A
SiO_2	22.71	23.02
TiO_2	0.41	0.64
Al_2O_3	59.62	58.68
FeO	12.28	14.41
MgO	1.60	1.93
ZnO	2.80	1.16
MnO	0.13	0.18
TOTAL	99.55	100.02
Formula moles, based on 23 oxygens		
Si	3.12	3.17
Zn	0.29	0.12
Al	9.70	9.54
Ti	0.04	0.07
Fe	1.42	1.66
Mg	0.33	0.40
Mn	0.02	0.02
TOTAL	23.45	22.95

Table A.6. Representative hornblende (hb) and biotite (bi) analyses in amphibolitic rocks

Sample	A(hb)	CL(hb)	TC(hb)	A(bi)	CL(bi)	TC(bi)
SiO_2	43.44	44.68	43.10	36.85	37.65	37.46
TiO_2	0.18	2.07	0.40	1.66	1.71	1.75
Al_2O_3	15.75	11.74	16.05	17.96	16.85	17.32
FeO	14.84	13.57	14.79	15.09	16.08	17.62
MnO	0.18	0.00	0.21	0.09	0.03	0.16
MgO	9.21	11.11	9.36	13.85	13.21	13.13
Na_2O	1.28	1.28	1.33	0.33	0.16	0.25
K_2O	0.52	1.34	0.50	8.99	9.38	9.02
TOTAL	97.28	96.59	97.68	94.82	95.07	96.71
Formula moles, based on 23 oxygens				Formula moles, based on 24 oxygens		
Si	6.42	6.64	6.35	5.50	5.64	5.55
Al_{IV}	1.58	1.36	1.65	2.50	2.36	2.45
Al_{VI}	1.17	0.69	1.14	0.66	0.61	0.57
Ti	0.02	0.23	0.04	0.19	0.19	0.19
Fe	1.83	1.69	1.82	1.88	2.01	2.18
Mn	0.02	0.00	0.03	0.01	0.00	0.02
Mg	2.03	2.46	2.06	3.08	2.95	2.90
Na	0.37	0.37	0.38	0.10	0.05	0.07
K	0.10	0.25	0.09	1.71	1.79	1.70
TOTAL	15.42	15.41	15.45	15.64	15.60	15.64

Table A.7. Representative garnet(grt) and pyroxene(px) analyses in amphibolitic rocks

Sample	A(grt)	CL(grt)	TC(grt)	CL(px)	
SiO_2	39.02	38.49	38.29	SiO_2	53.48
Al_2O_3	21.86	21.66	21.96	TiO_2	0.00
FeO	24.92	26.83	26.83	Al_2O_3	1.42
MgO	6.44	5.43	5.15	FeO	8.66
MnO	0.63	0.82	1.17	MgO	13.89
CaO	7.07	6.73	6.70	MnO	0.11
				CaO	22.22
TOTAL	99.94	99.96	100.10		
				Total	99.78
Formula moles, based on 12 oxygens				Formula moles, based on 6 oxygens	
Si	3.01	3.00	2.99	Si	1.99
Al	1.99	1.99	2.02	Al_{IV}	0.01
Fe	1.61	1.75	1.75	Al_{VI}	0.05
Mg	0.74	0.63	0.60	Ti	0.00
Ca	0.59	0.56	0.56	Fe	0.27
Mn	0.04	0.05	0.08	Mg	0.77
				Mn	0.01
TOTAL	7.99	8.00	8.00	Ca	0.89
				Total	3.98

Table A.8. Representative plagioclase analyses in amphibolitic rocks

Sample	A	CL	TC
SiO_2	58.07	59.82	59.25
Al_2O_3	25.68	25.16	25.36
FeO	0.00	0.00	0.00
CaO	9.20	7.21	8.39
BaO	0.00	0.00	0.00
Na_2O	6.79	7.42	7.30
K_2O	0.08	0.25	0.11
TOTAL	99.75	99.86	100.41
Formula moles, based on 8 oxygens			
Si	2.60	2.67	2.68
Al	1.37	1.32	1.33
Ca	0.45	0.34	0.40
Ba	0.00	0.00	0.00
Na	0.59	0.64	0.63
K	0.00	0.01	0.01
Fe	0.01	0.00	0.00
TOTAL	5.00	5.00	5.01

VITA

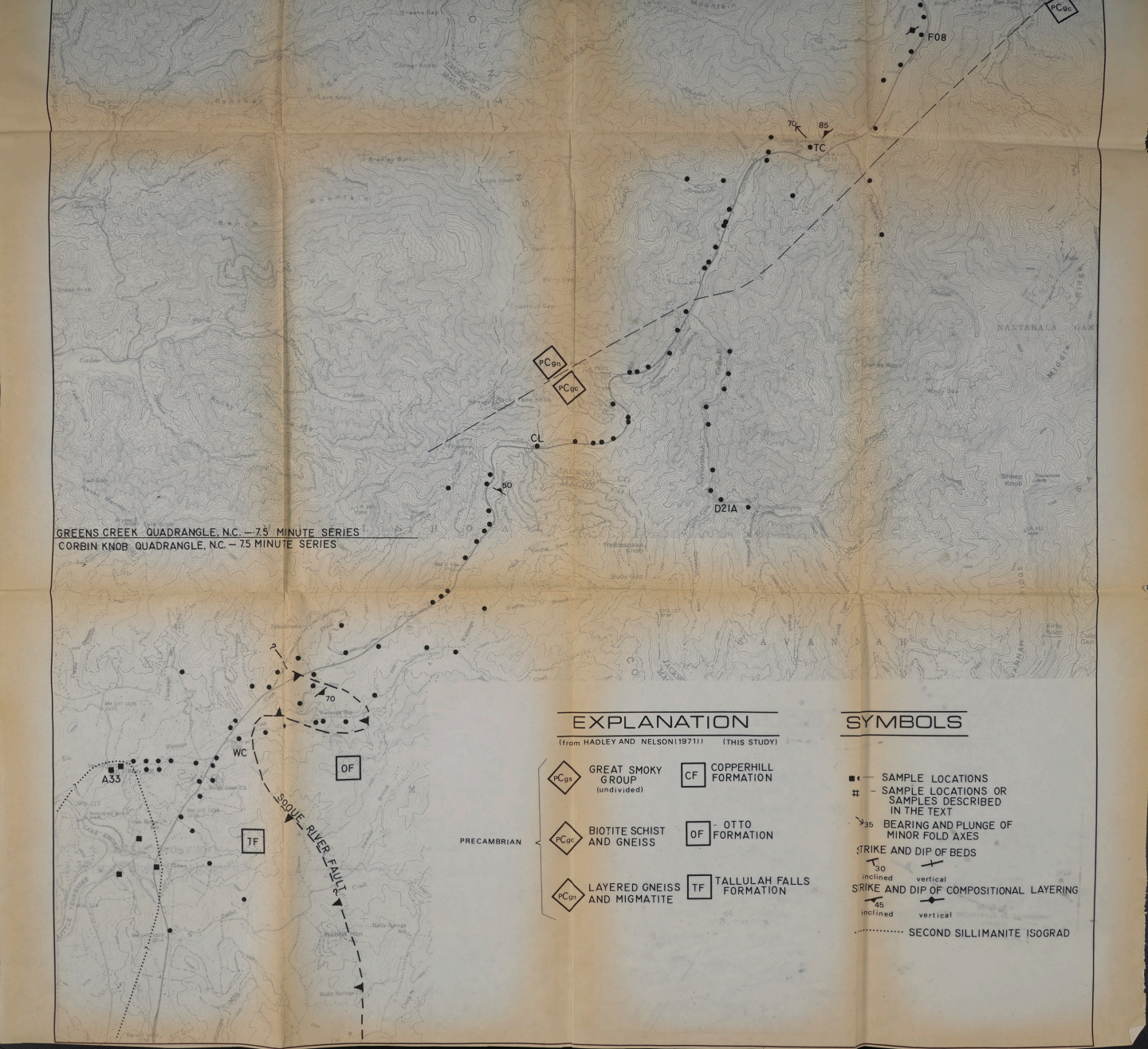
Vicki Jo Brumback was born in London, Kentucky on September 15, 1959. She attended elementary and secondary schools in Jackson County, Kentucky and was graduated from Jackson County High School in June 1977. The following September she entered Berea College in Berea, Kentucky, and in May 1981 she received a Bachelor of Arts degree in Earth Science. She received a secondary teaching certificate in December 1981, and from August 1982 through June 1984 taught science and math courses at Jackson County High School. In the fall of 1984 she enrolled in graduate school at the University of Tennessee-Knoxville and began study toward a Master's degree in geology. This degree was awarded in December 1990.

In the fall of 1987 she accepted a position as a subcontractor with Oak Ridge National Laboratory in Oak Ridge, Tennessee. She is currently employed as a geologist and risk analyst by Martin Marietta Energy Systems, Inc. in Oak Ridge National Laboratory's Office of Risk Analysis.

WHITTIER QUADRANGLE, N.C. — 7.5 MINUTE SERIES

GREENS CREEK QUADRANGLE, N.C. — 7.5 MINUTE SERIES




GREENS CREEK QUADRANGLE, N.C.—7.5' MINUTE SERIES
CORBIN KNOB QUADRANGLE, N.C. — 7.5 MINUTE SERIES
EXPLANATION
(from HADLEY AND NELSON(1971))
(THIS STUDY)
PRECAMBRIAN
PCgs GREAT SMOKY GROUP (undivided)
PCgc BIOTITE SCHIST AND GNEISS
PCgn LAYERED GNEISS AND MIGMATITE
CF COPPERHILL FORMATION
OF OTTO FORMATION
TF TALLULAH FALLS FORMATION
SYMBOLS
SAMPLE LOCATIONS
SAMPLE LOCATIONS OR SAMPLES DESCRIBED IN THE TEXT
35 BEARING AND PLUNGE OF MINOR FOLD AXES
STRIKE AND DIP OF BEDS
30 inclined
vertical
STRIKE AND DIP OF COMPOSITIONAL LAYERING
45 inclined
vertical
SECOND SILLIMANITE ISOGRAD
SOQUE RIVER FAULT
F08
TC
CL
D21A
A33
WC
OF
TF
PCgn
PCgc
NANTAHALA
GEORGIA
SOUTH CAROLINA